Université du Québec
Institute National de la Recherche Scientifique
(Énergie, Matériaux et Télécommunications)

Modelling Unequal Error Protection in BICM Systems

by
Thomas Chowdhury

A thesis submitted
in partial fulfillment of the requirements for the degree of
Master of Science

Supervisor : Prof. Leszek Szczecinski (INRS-EMT)
Internel Reviewer : Prof. Amar Mitiche (INRS-EMT)
External Reviewer : Prof. Adel Omar Dahmane
(Université du Québec à Trois-Rivières)

Montreal Canada

Abstract

Bit-interleaved coded modulation (BICM) is one of the popular modulation techniques used in most of the existing wireless communication standards, e.g., HSPA, IEEE 802.11a/g/n etc. In BICM, the channel encoder and the modulator are separated by a bit-level interleaver which allows the designer to choose the code rate and the constellation independently. BICM maximizes the code diversity, and therefore is better than trellis coded modulation in fading channel. However its flexibility and ease of implementation makes it popular in non-fading channel too.

In BICM, receiver considers the reliability metrics of the transmitted bit which are calculated in the form of log likelihood ratios (L-values) and the main goal of this research is to find the probabilistic model of L-values that allows for a simple and accurate evaluation of the performance of (BER) considering the effect of unequal error protection.

To this end we proceed in two steps. First we replace the exact form of the PDFs of L-values with simple to manipulate Gaussian functions. Next we interpret these simplified form into the BER evaluation based on the saddle point approximation. To deal with multiple terms appearing in the expressions which complicate the solution of the so-called saddlepoint equation; we use quadratic approximations which lead to the closed form solutions. The resulting formulas are validated in the case of M-QAM and M-PSK constellation with arbitrary labellings e.g. Gray, Set Partitioning (SP), Modified Set Partitioning Labelling (MSP) and Mixed labelling (ML).

Acknowledgement

My past few years as a graduate student is to ponder memories of great surprises, difficulties, depression, and successes fuelled by the immense passion for research. There are many people I would like to acknowledge for making my experience in INRS one of the most rewarding periods of my life. First of all, I would like to express my heartfelt gratitude to Professor Leszek Szczecinski. It would not be possible to produce this thesis without his friendly and generous support. I would like to thank Professor Szczecinski for his kindness and patience with enthusiasm to cultivate me not only in research but in life as well.

Moreover, I would like to thank all the members of the Communication group of INRS for their endless help. Specially I would like to thank Professor Douglas O'Shaughnessy for giving me the opportunity to write my thesis in English. For helping me with all the administrative tasks I would like to send my gratitude to Helene Sabourin and Nathalie Aguiar. My gratitude also goes to Sylvain Fauvel for arranging all the computer related stuff.

I am also very grateful to all of my friends in and out of INRS. I am indebted to them for sharing my joys and sorrows.

Finally but most importantly I would like to thank my parents for their love and blessings. I am grateful to my mother for raising me to an upright and caring person. I also thank to my elder sister and brother-in-law for always being there for me.

Chapitre 1

Résumé

Présentement, on ne peut pas imaginer la vie sans Internet. Les gens profitent de la vitesse de plusieurs dizaines de Mbps même en liaison sans fil, ce qui était un rêve quelques années avant. Les habitudes dans le travail et même plus généralement, toutes les façons dont nous interagissons ont été modifiées par la possibilité de communiquer “ n′importe où, à tout moment ” - répondre à des emails dans un café est devenu une activité commune. Un systéme de communication sans fil complexe fonctionne derriére ce scénario, il suit certaines normes de communication. Ces normes définissent comment des systémes de communication sont mis en œuvre pour répondre à la demande.

1.1 Introduction

La modulation codée par bit entrelacé (BICM) est une technique connue utilisée dans la plupart des normes existantes de communication sans fil par exemple HSPA [1], IEEE 802.11a/g/n, les normes DVB (DVB-T2 [15], DVB-S2 [16] et le DVB-C2 [17]). Le BICM-OFDM est également considéré comme un candidat potentiel pour les systémes de communication par ligne d′alimentation. La modulation codée par bit entrelacé a été introduite par la Zehavi dans [35]. L′avantage majeur du BICM est sa

simplicité et flexibilité, car un code binaire unique ne peut être utilisé avec plusieurs modulations sans d′autres adaptations. Le BICM maximise la diversité du code, il est donc meilleur que la modulation codée en trellis dans le canal à évanouissement. Dans cette, nous étudions les modèles probabilistes de mesures de fiabilité de la transmission du BICM qui permettent une évaluation simple et précise de la performance (TEB) en considérant les effets de la protection d′erreur inégale. Nous supposons que les paramétres de fiabilité du bit transmis sont calculés dans la forme de rapports de vraisemblance log (valeurs L) en utilisant une approximation max-log pour réduire la complexité mathématique [4], et nous proposons également une nouvelle approximation du point de selle qui est une des techniques populaires pour calculer la performance de BICM.

1.2 Modèlè de système

1.2.1 Convention de notation

Dans cette thèse, nous utilisons la lettre minuscule x pour désigner un scalaire, et la lettre $\boldsymbol{x}$ pour désigner une séquence. Le vecteur nul et le vecteur unitaire sont désignés par $\mathbf{0}$ et $\mathbf{1}$, respectivement. L′ensemble des nombres réels est noté par $\mathbb{R}$. Les variables aléatoires sont dénotées en lettres majuscules Y, les probabilités par $\Pr\{\cdot\}$, la fonction densité de probabilité (PDF) du vecteur aléatoire Y par $f(y)$. L′espérance d′une variable aléatoire Y est dénotée par $\mathbb{E}(Y)$. Une matrice est dénotée par $\mathbb{T}$. Un ensemble de symboles est dénoté par $\mathcal{X}$. Une distribution gaussienne avec une valeur moyenne μ et la variance σ^2 est dénoté par $\mathcal{N}_{\mu,\sigma^2}(\lambda)$, la fonction-erf par $erf(x) \triangleq \frac{2}{\sqrt{\pi}} \int_0^x \exp(-t^2)dt$ et la fonction échelon unité par $u(x) \triangleq \begin{cases} 1, & x \geq 0 \\ 0, & x < 0 \end{cases}$

1.2.2 Principes de BICM

Un système BICM est composé d′un encodeur binaire, un entrelaceur de bits (π) et un mappeur sans mémoire ($\mathcal{M}$) du côté de la transmission. La fonction du mappeur est de rendre les règles de correspondance biunivoques qui mappent les vecteurs binaires aléatoires de longueur $\boldsymbol{c}' = [c'_1, ..., c'_r]$ dans un symbole $\mathcal{X}$, c'est dire $\mathcal{M} : \{0,1\}^r \rightarrow \mathcal{X}$. Les symboles sont envoyés à travers le canal dont la sortie est donnée par $y = h \cdot x + \eta$ où h est le gain du canal complexe et η est un échantillon de bruit blanc Gaussien réel de variance N_0 et moyenne nulle. Comme le mappage est sans mémoire, tant le bruit comme les échantillons complexes du gain du canal sont indépendants et identiquement distribuées. Du côté du récepteur il existe une

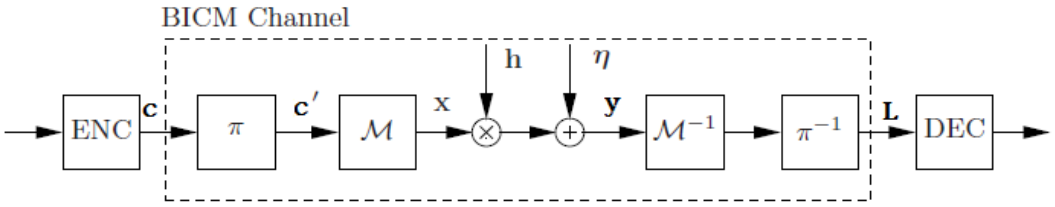

FIGURE 1.1: BICM modéle

concaténation en série du démappeur, désentrelaceur et un décodeur. La fonction du démappeur est de calculer les valeurs L et ensuite passer au de entrelaceur et au décodeur final. Alors les valeurs L peuvent être appelées comme indicateurs de fiabilité. Les mesures de fiabilité calculées par démappeur $\mathcal{M}^{-1}$ sont définies comme

$$\hat{L}_j = \log(\frac{\Pr\{c_j = 1|y\}}{\Pr\{c_j = 0|y\}}) \tag{1.1}$$

où y est un signal reçu, $j = 0, ..., r-1$ est la position du bit, et c_j est le bit j-ème dans le mot codé transmis $\boldsymbol{c} = [c_0, ..., c_{r-1}]$. Selon la régle de Bayes, il est possible

d′exprimer (1.1) comme une somme de valeurs L a priori extrinsèques.

$$\begin{aligned}\hat{L}_j &= \log(\frac{\Pr\{y|c_j=1\}}{\Pr\{y|c_j=1\}}) + \log(\frac{\Pr\{c_j=1\}}{\Pr\{c_j=1\}}) \\ &= L_j^{\mathrm{e}} + L_j^{\mathrm{a}}\end{aligned} \tag{1.2}$$

Où L_j^{a} est la probabilité a priori. Comme le canal est sans mémoire il n′y a pas d′information a priori, c′est à dire $(L_j^{\mathrm{a}} = 0)$ donc

$$\begin{aligned}\hat{L}_j &= \log(\frac{\Pr\{y|c_j=1\}}{\Pr\{y|c_j=1\}}) \\ &= \log\{\frac{\sum_{a\epsilon\mathcal{X}_{j,1}} \exp(-\gamma|\frac{y}{h}-a|^2)}{\sum_{a\epsilon\mathcal{X}_{j,0}} \exp(-\gamma|\frac{y}{h}-a|^2)}\}\end{aligned} \tag{1.3}$$

L′équation (1.3) peut être simplifié en utilisant une approximation max-log. Alors la forme simplifiée de l′équation est donnée ci-dessous

$$L_j = \min_{a\epsilon\mathcal{X}_{j,0}}(\gamma|\frac{y}{h}-a|^2) - \min_{a\epsilon\mathcal{X}_{j,1}}(\gamma|\frac{y}{h}-a|^2) \tag{1.4}$$

1.2.3 Étiquetages binaires

Un $\mathbb{T}$ étiquetage binaire est defini en utilisant une matrice de dimensions $M = 2^r$ par r, où chaque ligne correspond à mots binaires distincts de longueur r M , $\mathbb{L} \triangleq [c_1^T, ..., c_M^T]^T$, où $\boldsymbol{c}_i = [c_{i,1}, c_{i,2}, ..., c_{i,r}]\epsilon\{0,1\}^r$. Nous sommes particulièrement intéressés par le code Gray binaire reflechi (BRGC), Set-partitionnement (SP), le partitionnement modifié Set (MSP) et étiquetage-mixte (ML). Figure 1.2, 1.3 montrent la représentation graphique de ces étiquetages populaires.

1.2.4 Modèle de Canal

Les modèles de canal peuvent être définis comme des modèles de canal continu puisqu′il n′y a pas une limite pour la précision que leurs valeurs peuvent avon. Selon la théorie de l′information, il s′agit d′une approche commune que de commencer par les canaux sans mémoire dans lequel la distribution de probabilité de sortie ne repose

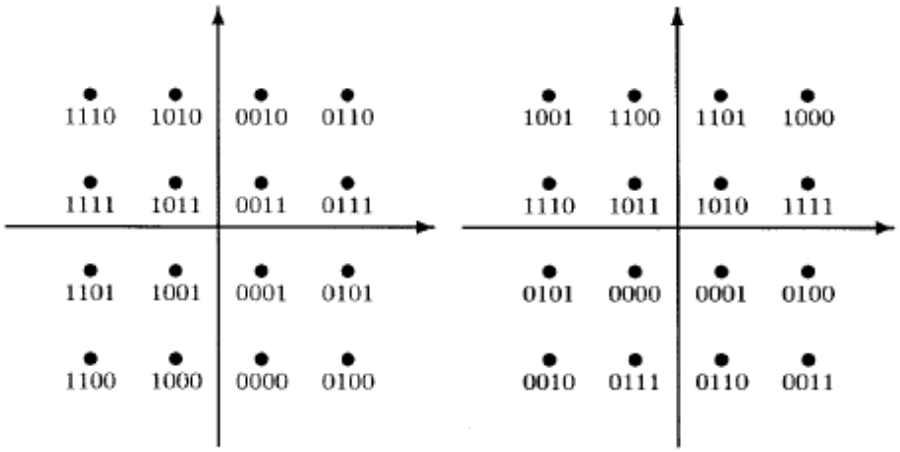

(a) (b)

FIGURE 1.2: (a) Étiquetages Gray et (b) étiquetages Set partitionnement [11]

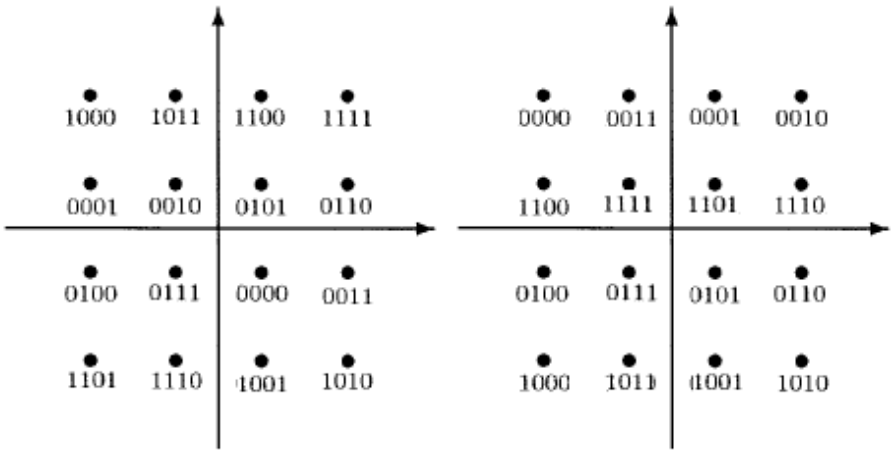

(a) (b)

FIGURE 1.3: (a) Étiquetages Modifié Set-partitionnement et (b) étiquetages étiquetage-mixte [12]

que sur le canal d'entrée actuel. Un modèle de canal peut être soit numérique (quantifié, par exemple binaire) ou analogique. Dans le monde réel, la transmission est toujours affectée par le bruit. Le modèle mathématique habituel est le canal AWGN (bruit blanc gaussien additif). Le bruit AWGN est un processus Gaussien aléatoire stationnaire de moyenne nulle [25]. Cela signifie que la sortie de chaque mesure du bruit est une variable aléatoire Gaussienne de moyenne nulle qui ne dépend pas de l'instant du temps où la mesure est faite. Le signal de bande passante transmis x est corrompue par le AWGN, résultant le signal reçu

$$y = x + \eta \tag{1.5}$$

où η est un bruit blanc Gaussien.
Après avoir traversé le canal évanoui, le signal reçu est atténué au niveau du récepteur par le bruit blanc gaussien additif qui est supposé être statistiquement indépendant de la fluctuation d'amplitude h et se caractérise par une densité de puissance spectrale unilatérale N_0 [25]. Le signal reçu peut être représenté comme

$$y = h \cdot x + \eta \tag{1.6}$$

Puis le rapport signal bruit (SNR) peut être défini comme

$$\gamma = h^2 \frac{E_s}{N_0}$$

Et la moyenne du signal bruit (SNR) est

$$\bar{\gamma} = \mathbb{E}[h^2] \frac{E_s}{N_0}$$

où E_s est l'énergie par symbole et $\mathbb{E}[h^2]$ est la puissance de fluctuation moyenne.

La distribution de Rayleigh est principalement utilisé pour modeler l'évanouissement sans ligne de vue (LOS). Le SNR instantané par symbole γ est distribué selon la distribution suivante [28].

$$f_{\bar{\gamma}}(\gamma) = \frac{1}{\bar{\gamma}} \exp(-\frac{\gamma}{\bar{\gamma}}), \gamma \geq 0 \tag{1.7}$$

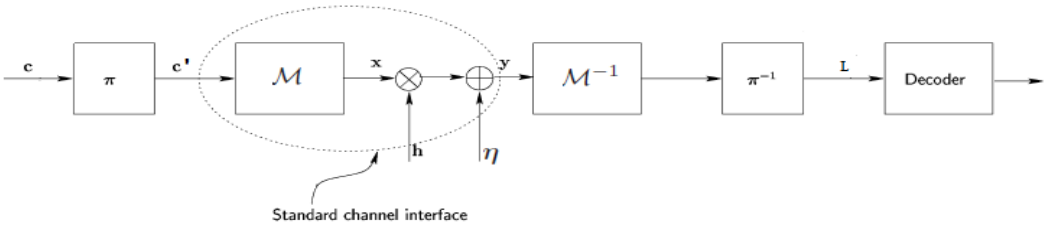

FIGURE 1.4: BICM canal de transmission

La fonction de distribution de probabilité Nakagami-m peut être exprimée comme SNR par symbole, qui est distribuée selon la distribution gamma [28].

$$f_{\bar{\gamma}}(\gamma) = \frac{m^m \gamma^{m-1}}{\bar{\gamma}^m \Gamma(m)} \exp(-\frac{m\gamma}{\bar{\gamma}}) \tag{1.8}$$

1.3 Modèle Probabiliste

Les L-values peuvent être considérées comme la sortie du canal BICM qui est la combinaison d′entrelaceur, modulateur, le canal de transmission, de démodulation et de-entrelaceur [22] En supposant un fonctionnement avec les idéaux d′entrelacement, est considéré comme sans mémoire [35]. La PDF de la L-values peut être exprimée comme la somme pondérée des PDFs $f_{L|j,x,\gamma}(\lambda)$ conditionnée à la position du bit $1 \leq j \leq r$ et du symbole transmis $x \epsilon \mathcal{X}_{j,1}$ [20].

$$\begin{aligned} f_{L|c=1,\gamma}(\lambda) &= \frac{1}{r} \sum_{j=1}^{r} \sum_{x \epsilon \mathcal{X}_{j,1}} Pr(x|c=b,j) f_{L|j,x,\gamma}(\lambda) \\ &= \frac{1}{r 2^{r-1}} \sum_{k=1}^{r} \sum_{x \epsilon \mathcal{X}_{k,1}} f_{L|j,x,\gamma}(\lambda) \end{aligned} \tag{1.9}$$

La PDF des L values de M-QAM en considerant la transmission de $c = 1$ en remplaçant la $f_{L|j,x,\gamma}(\lambda)$ dans (1.9) $f_{L,k|\gamma,d_l}(\lambda)$, de table de 1.1, peut être exprimée comme [20].

$$\begin{aligned} f_{L|\gamma}^{\text{QAM}}(\lambda) &= \frac{1}{r 2^{r-1}} \sum_{k=1}^{5} \sum_{l=1}^{2^{r-1}-1} n_{k,l} f_{L,k|\gamma,d_l}(\lambda) \\ d_l &= l d_{\min} \end{aligned} \tag{1.10}$$

Et la PDF des L-values pour la constellation M-PSK peut être écrite comme [20].

$$
\begin{aligned}
f_{L|\gamma}^{\mathrm{PSK}}(\lambda) &= \frac{1}{r2^{r-1}} \sum_{l=1}^{2^{r-1}-1} [n_{1,l} f_{L,1|\gamma,d_l}(\lambda) + n_{6,l} f_{L,6|\gamma,d_l,\theta_l}(\lambda)] \\
d_l &= \frac{\sin(\frac{\pi l}{2^r})}{\sin(\frac{\pi}{2^r})} d_{\min} \\
\theta_l &= \pi - \frac{2\pi l}{2^r}
\end{aligned}
\tag{1.11}
$$

Les fonctions PDF sont calculées compte tenu des sous-ensembles de points de signal concurrentiel à savoir $c = 0$ à une distance d_l. Le coefficient $n_{k,l}$ indique le nombre de sous-ensembles de type k à une distance d_l. Le tableau 1.2 montre les valeurs numériques des $n_{k,l}$ pour des constellations bien connues et des règles d'étiquetage.

TABLE 1.1: La fonction de densité de probabilité de fiabilité $f_{L,k|\gamma,d_l}(\lambda)$ et $f_{L,k|\gamma,d_l,\theta_l}(\lambda)$ pour la transmission sur le canal AWGN

$k = 1$	$\mathcal{N}_{d^2\gamma,2d^2\gamma}(\lambda)$
$k = 2$	$\mathcal{N}_{d^2\gamma,2d^2\gamma}(\lambda)(1 - erf(\frac{\lambda - d^2\gamma}{2d\sqrt{\gamma}}))$
$k = 3$	$2\mathcal{N}_{d^2\gamma,2d^2\gamma}(\lambda)u(d^2\gamma - \lambda)$
$k = 4$	$\mathcal{N}_{d^2\gamma,2d^2\gamma}(\lambda)(1 - 2erf(\frac{\lambda - d^2\gamma}{2d\sqrt{\gamma}}))u(d^2\gamma - \lambda)$
$k = 5$	$-4\mathcal{N}_{d^2\gamma,2d^2\gamma}(\lambda)erf(\frac{\lambda - d^2\gamma}{2d\sqrt{\gamma}})u(d^2\gamma - \lambda)$
$k = 6$	$\mathcal{N}_{d^2\gamma,2d^2\gamma}(\lambda)(1 - erf(\tan(\frac{\theta}{2})\frac{\lambda - d^2\gamma}{2d\sqrt{\gamma}}))$

la fonction erf peut être exprimée comme

$$
erf(\alpha) \approx \begin{cases} 1 - \exp(-\alpha^2); & \alpha > 0 \\ \exp(-\alpha^2) - 1; & \alpha < 0 \end{cases}
\tag{1.12}
$$

Les PDF du tableau 1.1 peuvent être redefinies comme pour simplifier l'évaluation des performances du BICM. Il s'agit d'utiliser la transformée de Laplace de la PDF

TABLE 1.2: Valeurs du coefficient $n_{k,l}$ pour un nombre populaires de constellation et étiquetage. Seuls les coefficients non nuls sont affichés

4QAM	GL	$n_{1,1} = 4$
	SPL	$n_{1,1} = 2, n_{2,1} = 2$
16QAM	GL	$n_{1,1} = 24, n_{1,2} = 8$
	SPL	$n_{1,1} = 8, n_{1,2} = 4, n_{2,1} = 10, n_{3,1} = 4, n_{4,1} = 4, n_{5,1} = 2$
	MSPL	$n_{1,1} = 16, n_{2,1} = 4, n_{2,2} = 2, n_{3,1} = 4, n_{4,1} = 4, n_{5,1} = 2$
	ML	$n_{1,1} = 24, n_{3,1} = 8$
64QAM	GL	$n_{1,1} = 112, n_{1,2} = 48, n_{1,3} = 16, n_{1,4} = 16$
8PSK	GL	$n_{1,1} = 8, n_{1,2} = 4$
	SPL	$n_{1,1} = 6, n_{1,2} = 2, n_{2,1} = 4$
	SSPL	$n_{1,1} = 6, n_{2,1} = 6$

des L-values.

$$\begin{aligned}\Phi_{L|c=1,\bar{\gamma}}(s) &= \int_{-\infty}^{\infty} f_{L|c=1,\bar{\gamma}}(\lambda)\exp(-s\lambda)d\lambda \\ &= \int_{0}^{\infty}\left(\int_{-\infty}^{\infty} f_{L|c=1,\gamma}(\lambda)\exp(-s\lambda)d\lambda\right) f_{\bar{\gamma}}(\gamma)d\gamma \\ &= \int_{0}^{\infty}\Phi_{L|c=1,\gamma}(s) f_{\bar{\gamma}}(\gamma)d\gamma\end{aligned} \tag{1.13}$$

où $\Phi_{L|c=1,\gamma}(s)$ est la transformée de Laplace du PDF sur le canal AWGN et nous supposons $s\epsilon\mathbb{R}^{+}$. Le tableau 1.4 présente la transformée de Laplace de la PDF de six sous-ensembles non-équivalent de points de signal concurrentiel sur AWGN canal et Nakagami-m canal fading

1.3.1 Taux d′erreur d′approximation à l′aide de l′Union Bound

Pour prouver l′exactitude du modèle approximatif, nous utilisons ce modèle pour calculer les limites sur le BER dans une transmission codé. Union limite sur le BER

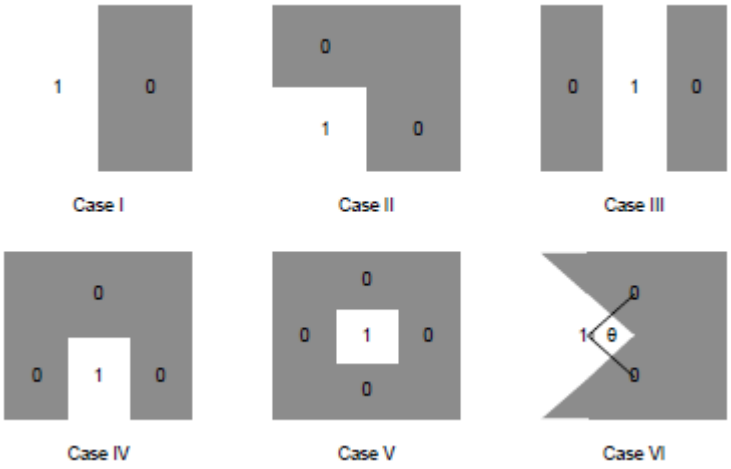

FIGURE 1.5: Six formations non-équivalentes pour l'ensemble des points de signaux concurrentiels. Le '1' représente le point de signal transmis et les '0' montrent les éléments du point de signal concurrentiel [20]

dans une transmission codée peut être écrite comme [32]

$$P_{\mathrm{b}} \leq UB = \sum_{d=d_{\mathrm{free}}}^{\infty} \beta_d \cdot PEP(d) \tag{1.14}$$

d_{free} est la distance libre du code, β_d est le spectre de la distribution du poids du code et de la $PEP(d)$ est la probabilité d'erreur par paires qui indique. Probabilité de détecter un mot de code avec le poids (distance) de Hamming égale à d au lieu de transmettre tout dans un seul mot de code. Les L-valeurs sont entrelacées, par conséquent, elles sont indépendantes. Donc la sommation de leur PDF la convolution de chacune d'entre eux, exprimée par

$$f_{L|c,\gamma}^{\sum_d}(\lambda) = f_{L|c,\gamma}(\lambda) * f_{L|c,\gamma}(\lambda) * ... * f_{L|c,\gamma}(\lambda) \tag{1.15}$$

La probabilité d'erreur par paire est égale à l'intégrale de PDF résultant dans le canal AWGN

$$PEP(d) = \int_{-\infty}^{0} f_{L|c,\gamma}^{\sum_d}(\lambda) d\lambda \tag{1.16}$$

TABLE 1.3: Nouvelle fonction de densité de probabilité de fiabilité métriques $f_{L,k|\gamma,d_l}(\lambda)$ et $f_{L,k|\gamma,d_l,\theta_l}(\lambda)$ pour la transmission sur le canal AWGN

$k=1$	$\mathcal{N}_{d^2\gamma,2d^2\gamma}(\lambda)$
$k=2$	$2\mathcal{N}_{d^2\gamma,2d^2\gamma}(\lambda)-\frac{1}{\sqrt{2}}\mathcal{N}_{d^2\gamma,d^2\gamma}(\lambda)$
$k=3$	$2\mathcal{N}_{d^2\gamma,2d^2\gamma}(\lambda)$
$k=4$	$3\mathcal{N}_{d^2\gamma,2d^2\gamma}(\lambda)-\sqrt{2}\mathcal{N}_{d^2\gamma,d^2\gamma}(\lambda)$
$k=5$	$4\mathcal{N}_{d^2\gamma,2d^2\gamma}(\lambda)-2\sqrt{2}\mathcal{N}_{d^2\gamma,d^2\gamma}(\lambda)$
$k=6$	$2\mathcal{N}_{d^2\gamma,2d^2\gamma}(\lambda)-\cos(\frac{\theta}{2})\mathcal{N}_{d^2\gamma,2\cos^2(\frac{\theta}{2})d^2\gamma}(\lambda)$

Si $\Phi_{L,c|\bar{\gamma}}(s)$ est la transformée de Laplace de PDF d'une métrique fiable, l'expression mathématique de PDF(d) devient

$$PEP(d)=\frac{1}{2\pi j}\int_{\alpha-j\infty}^{\alpha+j\infty}[\Phi_{L,c|\bar{\gamma}}(s)]^d\frac{ds}{s} \tag{1.17}$$

Où $j\triangleq\sqrt{-1}$ et $\alpha\epsilon\mathbb{R}$ sont déterminées dans la région de convergence de l'intégrale. La partie gauche de l'équation (1.17) est réelle, ce qui impose que la partie droite doit être aussi réelle. Donc en remplaçant s par $\alpha+j\omega$

$$PEP(d)=\frac{1}{2\pi}\int_{-\infty}^{\infty}\frac{\alpha\Re[\Phi_{L,c|\bar{\gamma}}(\alpha+j\omega)^d]+\omega\Im[\Phi_{L,c|\bar{\gamma}}(\alpha+j\omega)^d]}{\alpha^2+\omega^2}d\omega \tag{1.18}$$

On peut utiliser la formule de l'intégrale de Gauss Hermite pour résoudre cette équation. Selon l'intégrale de Gauss Hermite on a

$$\int_{-\infty}^{\infty}h(q)dq\simeq\sum_{i=1}^{n}p_i\exp(q_i^2)h(q_i) \tag{1.19}$$

Où $h(q)=\exp(-q^2)\Phi_{L,c|\bar{\gamma}}(q)$, p_i est le poids et n est le nœud total.

1.3.1.1 Résultats numériques

Pour montrer l'exactitude de notre approche, on compare les résultats obtenus par l'approximation à ceux obtenus par une évaluation numérique. Pour calculer le

TABLE 1.4: La fonction de densité de probabilité de fiabilité métriques $\Phi_{L,k|\gamma,d_l}(s)$, $\Phi_{L,k|\gamma,d_l,\theta_l}(s)$, $\Phi_{L,k|\bar{\gamma},d_l}(s)$, et $\Phi_{L,k|\bar{\gamma},d_l,\theta_l}(s)$

$k=1$	$\Phi_{L,1\|d,\gamma}(s)$	$\exp(d^2\gamma(s^2-s))$
	$\Phi_{L,1\|d,\bar{\gamma}}(s)$	$\left(\frac{m}{m-d^2\bar{\gamma}(s^2-s)}\right)^m$
$k=2$	$\Phi_{L,2\|d,\gamma}(s)$	$2\exp(d^2\gamma(s^2-s)) - \frac{1}{\sqrt{2}}\exp(d^2\gamma(\frac{s^2}{2}-s))$
	$\Phi_{L,2\|d,\bar{\gamma}}(s)$	$2\left(\frac{m}{m-d^2\bar{\gamma}(s^2-s)}\right)^m - \frac{1}{\sqrt{2}}\left(\frac{m}{m-d^2\bar{\gamma}(\frac{s^2}{2}-s)}\right)^m$
$k=3$	$\Phi_{L,3\|d,\gamma}(s)$	$2\exp(d^2\gamma(s^2-s))$
	$\Phi_{L,3\|d,\bar{\gamma}}(s)$	$2\left(\frac{m}{m-d^2\bar{\gamma}(s^2-s)}\right)^m$
$k=4$	$\Phi_{L,4\|d,\gamma}(s)$	$3\exp(d^2\gamma(s^2-s)) - \sqrt{2}\exp(d^2\gamma(\frac{s^2}{2}-s))$
	$\Phi_{L,4\|d,\bar{\gamma}}(s)$	$3\left(\frac{m}{m-d^2\bar{\gamma}(s^2-s)}\right)^m - \sqrt{2}\left(\frac{m}{m-d^2\bar{\gamma}(\frac{s^2}{2}-s)}\right)^m$
$k=5$	$\Phi_{L,5\|d,\gamma}(s)$	$4\exp(d^2\gamma(s^2-s)) - 2\sqrt{2}\exp(d^2\gamma(\frac{s^2}{2}-s))$
	$\Phi_{L,5\|d,\bar{\gamma}}(s)$	$4\left(\frac{m}{m-d^2\bar{\gamma}(s^2-s)}\right)^m - 2\sqrt{2}\left(\frac{m}{m-d^2\bar{\gamma}(\frac{s^2}{2}-s)}\right)^m$
$k=6$	$\Phi_{L,6\|d,\theta,\gamma}(s)$	$2\exp(d^2\gamma(s^2-s)) - \cos(\frac{\theta}{2})\exp(d^2\gamma(\cos^2(\frac{\theta}{2})s^2-s))$
	$\Phi_{L,6\|d,\theta,\bar{\gamma}}(s)$	$2\left(\frac{m}{m-d^2\bar{\gamma}(s^2-s)}\right)^m - \cos(\frac{\theta}{2})\left(\frac{m}{m-d^2\bar{\gamma}(\cos^2(\frac{\theta}{2})s^2-s)}\right)^m$

BER, on suppose que BICM a un taux de convolution de code égale à 1, le polynôme générateur est $[5\ 7]_8$ de longueur constante égal à $K = 3$. D′abord on présente les résultats pour un canal AWGN puis on les représente pour un canal à évanouissement Nakagami-m. Pour le calcul de BER (union bound), on considère uniquement les 20 premiers termes de la représentation spectrale de la distance du code de convolution.

La figure 1.6 présente la comparaison des résultats exactes de BER comparés à ceux obtenus par l′approximation dans un canal AWGN pour les constellations 8PSK et 16QAM. On remarque que le BER (union bound) se trouve entre le modèle exacte et le modèle approximatif et surtout pour les valeurs inférieures à 10^{-4}. Donc l′approximation donne des résultats bien de BICM dans le canal AWGN. Dans la figure 1.7 et 1.8, on montre la comparaison entre les résultats exactes et approximés de BER dans la canal Nakagami-m en fonction de SNR. On peut notre que la bonde d′union du BER est entre le modèle exact et la modèle approximatif dans la majorité de la region SNR et dans le cas de resultats simulés il est particulierment au 10^{-4}. Par consèquent, le modèle approximtif prédit bien la performance du taux d′erreur de BICM sur le canal fading Nakagami-m.

1.4 Approximation du point Selle

Le PEP peut être exprimé comme la probabilité que de variable aleátoire générée en additionnant d LLRs $L_1, L_2, ..., L_d$. Il peut être exprimé en choisissant l′ensemble de mots de code comme étant un mot de code de référence

$$PEP(d) = Pr(L^{\sum_d} \triangleq \sum_{i=1}^{d} L_i < 0) \tag{1.20}$$

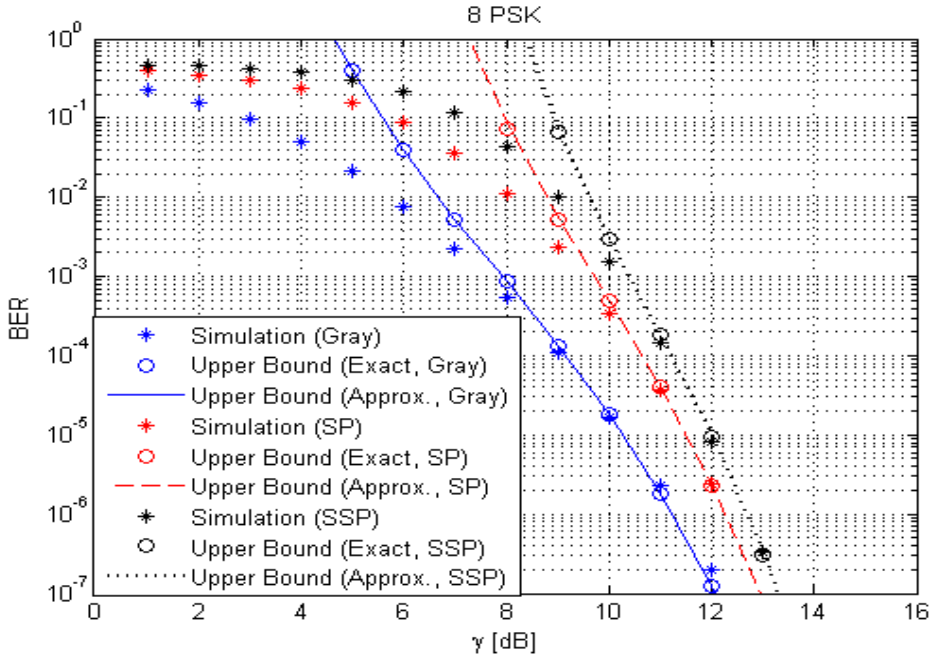

(a)

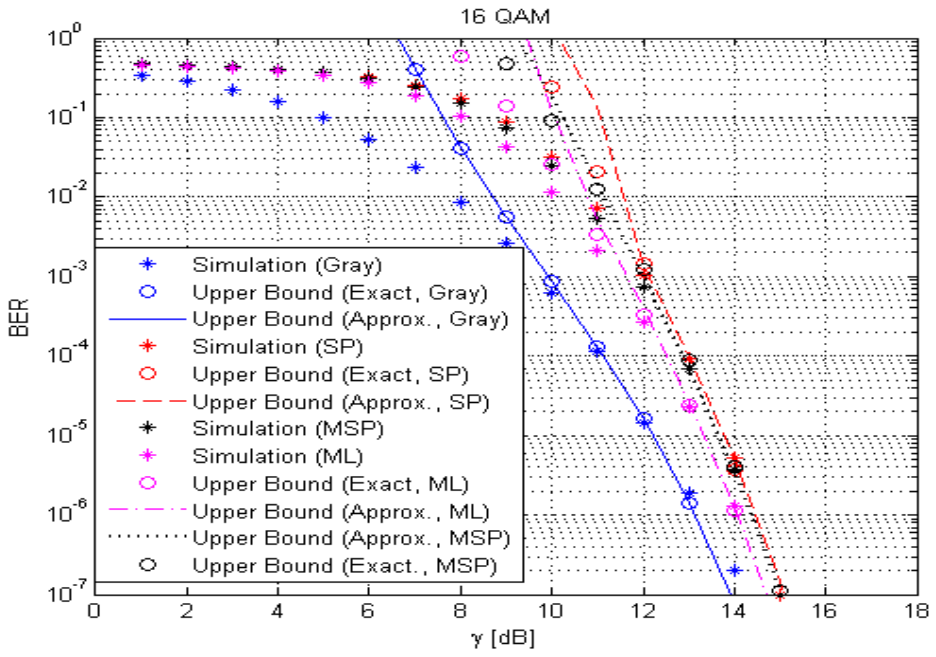

(b)

FIGURE 1.6: BER de la transmission sur le canal AWGN BICM pour un code convolutif de taux de $\frac{1}{2}$

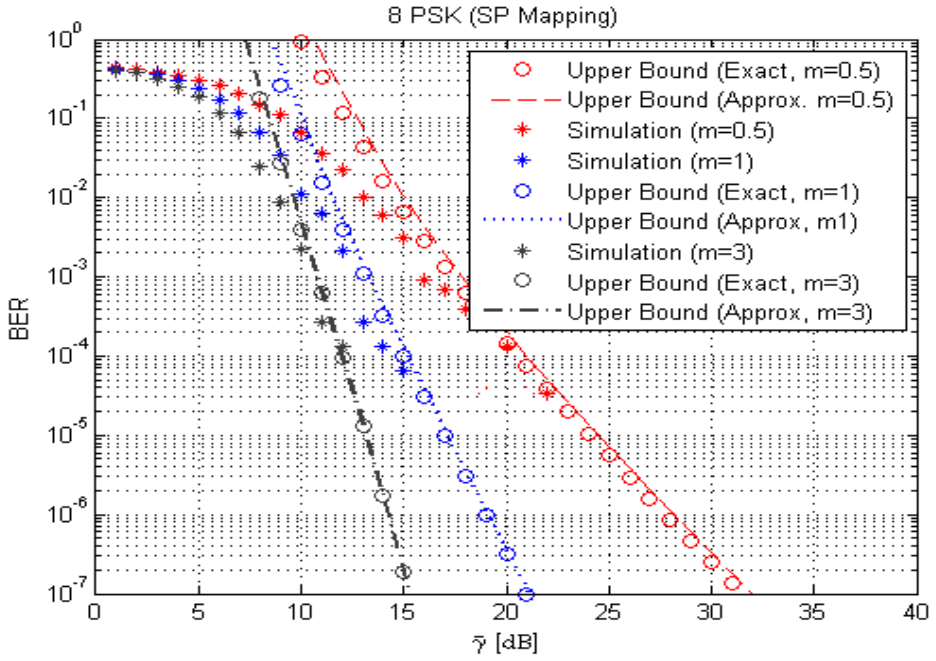

(a)

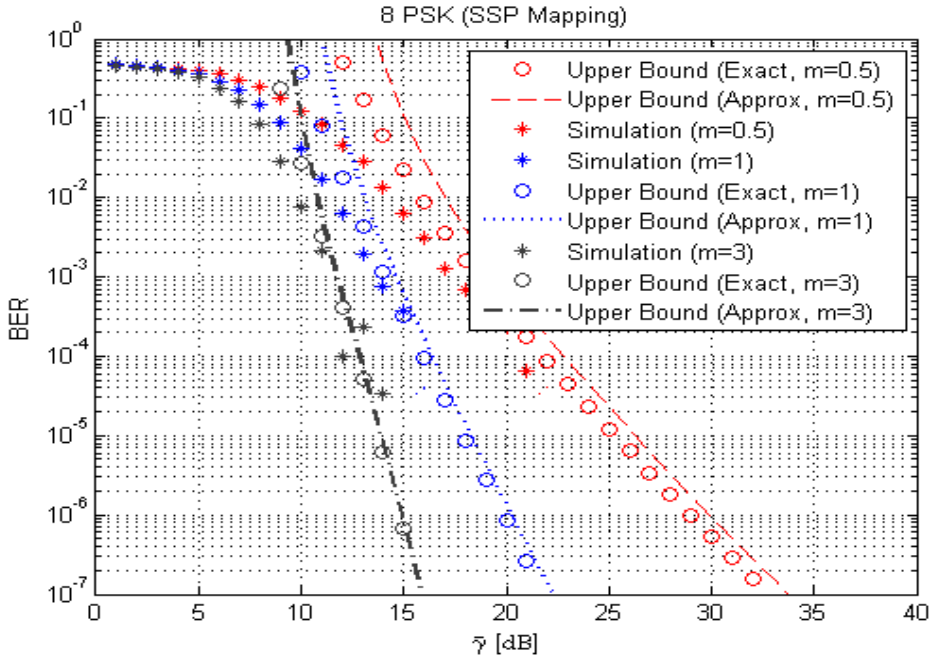

(b)

FIGURE 1.7: BER de la transmission du BICM plus Nakagami-m de canal pour un code de convolution de taux de $\frac{1}{2}$ pour 8 PSK

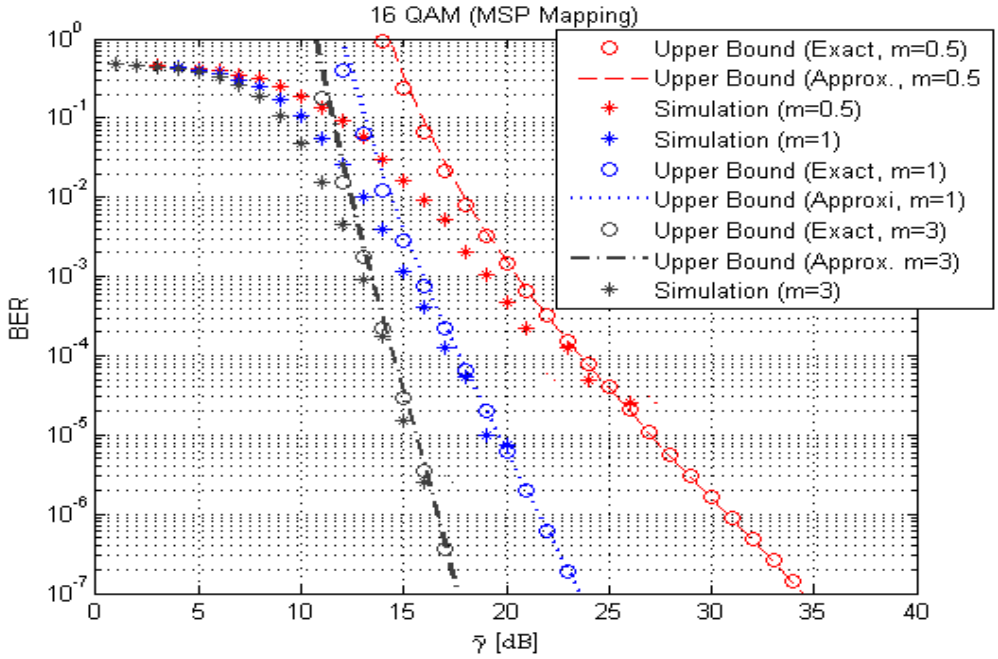

(a)

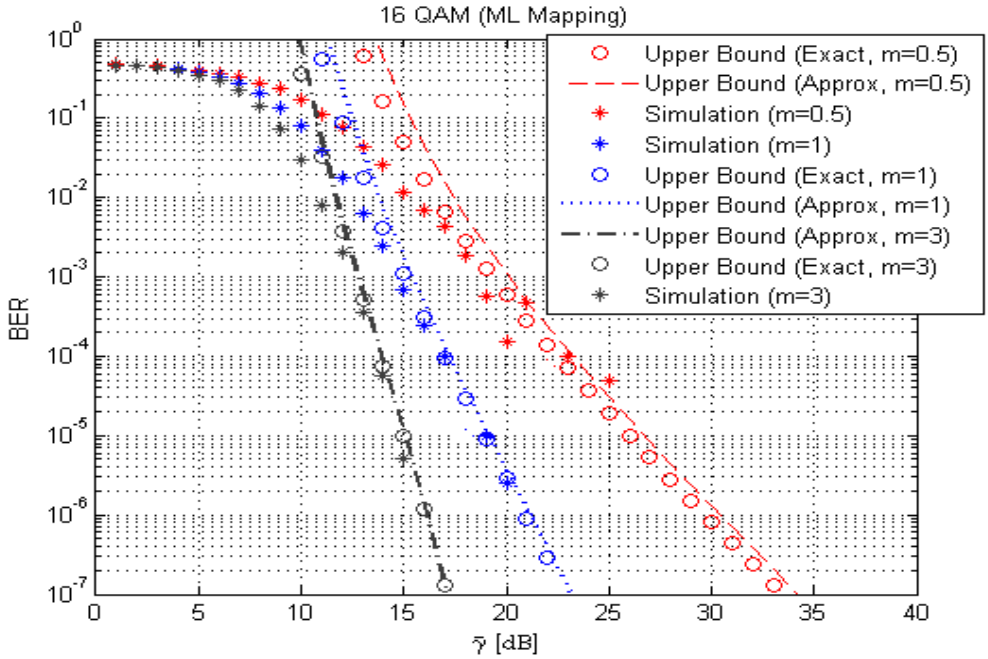

(b)

FIGURE 1.8: BER de la transmission du BICM plus Nakagami-m de canal pour un code de convolution de taux de $\frac{1}{2}$ pour 16 QAM

La transformation de Laplace de la PDF totale des d valeurs de L peut être écrite comme suit

$$\begin{aligned}\Phi_{d|\bar{\gamma}}^{\sum_d}(s) &= \prod_{i=1}^{d} \Phi_{d|L_i,\bar{\gamma}}(s) \\ &= [\Phi_{d|L,\bar{\gamma}}(s)]^d\end{aligned}$$

avec $\Phi_{d|L,\bar{\gamma}}(s)$ est la transformation de Laplace de chaque valeur de L. L'expression mathématique pour calculer l'approximation du point selle peut être exprimée comme suit

$$PEP(d) = \frac{\exp(\kappa_{d|\bar{\gamma}}(\hat{s}))}{\hat{s}\sqrt{2\pi\kappa_{d|\bar{\gamma}}^{''}(\hat{s})}} \tag{1.21}$$

avec $\kappa_{d|\bar{\gamma}}(s)$ est la fonction de génératrice des cumulantes et $\hat{s}$ est le point de selle defini par la derivé première $\kappa_{d|\bar{\gamma}}^{'}(\hat{s}) = 0$. La fonction de génération cumulante de la PDF est exprimée comme suit

$$\kappa_{d|\bar{\gamma}}(s) = d\log(\Phi_{d|L,\bar{\gamma}}(s)) \tag{1.22}$$

La dérivée première de $\kappa_{d|\bar{\gamma}}(s)$ par rapport à s est écrite comme suit

$$\kappa_{d|\bar{\gamma}}^{'}(s) = \frac{d\Phi_{d|L,\bar{\gamma}}^{'}(s)}{\Phi_{d|L,\bar{\gamma}}} \tag{1.23}$$

et la dérivée seconde de $\kappa_{d|\bar{\gamma}}(s)$ par rapport à s est exprimée comme suit

$$\kappa_{d|\bar{\gamma}}^{''}(s) = \frac{d\Phi_{d|L,\bar{\gamma}}^{''}(s)}{\Phi_{d|L,\bar{\gamma}}(s)} - \frac{d[\Phi_{d|L,\bar{\gamma}}^{'}(s)]^2}{[\Phi_{d|L_i,\bar{\gamma}(s)}]^2} \tag{1.24}$$

En remplaçant la valeur de $\kappa_{d|\bar{\gamma}}(s)$ et $\kappa_{d|\bar{\gamma}}^{''}(s)$ dans (1.25), l'expression mathématique de $PEP(d)$ sera

$$PEP(d) = \frac{[\Phi_{d|L,\bar{\gamma}}(\hat{s})]^{d+\frac{1}{2}}}{\hat{s}\sqrt{2\pi\Phi_{d|L,\bar{\gamma}}^{''}(\hat{s})}} \tag{1.25}$$

A partir (1.10,1.11), on peut savoir que la PDF des métriques de fiabilité est composée de plus d'un composent Gaussien. Si la transformation de Laplace de la PDF

totale $\Phi_{d|L,\bar{\gamma}}(s)$, et le termes Gaussien de la PDF totale sont $\Phi_1(s), ..., \Phi_n(s)$, alors l'expression mathematique de la PDF totale peut écrite sous la forme

$$\Phi_{d|L,\bar{\gamma}}(s) = \sum_{i=1}^{n} \Phi_i(s) \tag{1.26}$$

Selon rapprochement point selle, $\kappa^{'}(\hat{s}) = \Phi^{'}_{d|L,\bar{\gamma}}(\hat{s}) = 0$. Nous avons donc besoin de résoudre

$$\sum_{i=1}^{n} \Phi^{'}_i(\hat{s}) = 0 \tag{1.27}$$

Au lieu de le résoudre directement, ce qui peut être difficile, nous avons propośee l'approximation pour simplifier le problème. Maintenant, si nous considérons $\hat{s}_i$ est le point de selle en définissant la dérivée première de la i-th transformée de Laplace Gaussien terme $\Phi^{'}_i(\hat{s}_i) = 0$ alors d'après le théorème de Taylor [24].

$$\Phi^{'}_i(\hat{s}) \approx \Phi^{'}_i(\hat{s}_i) + (\hat{s} - \hat{s}_i)\Phi^{''}_i(\hat{s}_i) \tag{1.28}$$

Remplacement de la valeur de $\Phi^{'}_i(\hat{s})$ dans (1.27) nous obtenons

$$\begin{aligned} \sum_{i=1}^{n} (\hat{s} - \hat{s}_i)\Phi^{''}_i(\hat{s}_i) &= 0 \\ \hat{s} &= \frac{\sum_{i=1}^{n} \hat{s}_i \Phi^{''}_i(\hat{s}_i)}{\sum_{i=1}^{n} \Phi^{''}_i(\hat{s}_i)} \end{aligned} \tag{1.29}$$

1.4.1 Résultats numériques

On compare les résultats numérique avec le modèle exact afin de prouver l'exactitude de l'approximation proposée pour calculer le point selle. Pour calculer le BER, on suppose le BICM avec un taux de code convolutionnel égale à $\frac{1}{2}$ et avec un générateur polynomial $[5\ 7]_8$ avec une contrainte de longueur $K = 3$. Tout d'abord, on considère les rèsultats BER sur le canal fading Nakagami-m. Cependant, on considère les 20 premiers termes de la distance spectacale du code convolutionnel. La figure 1.9 et 1.10 montrent que les courbes du BER sont obtennues en utilisant l'approximation du point selle avec une nouvelle approximation pour trouver le point de selle et en

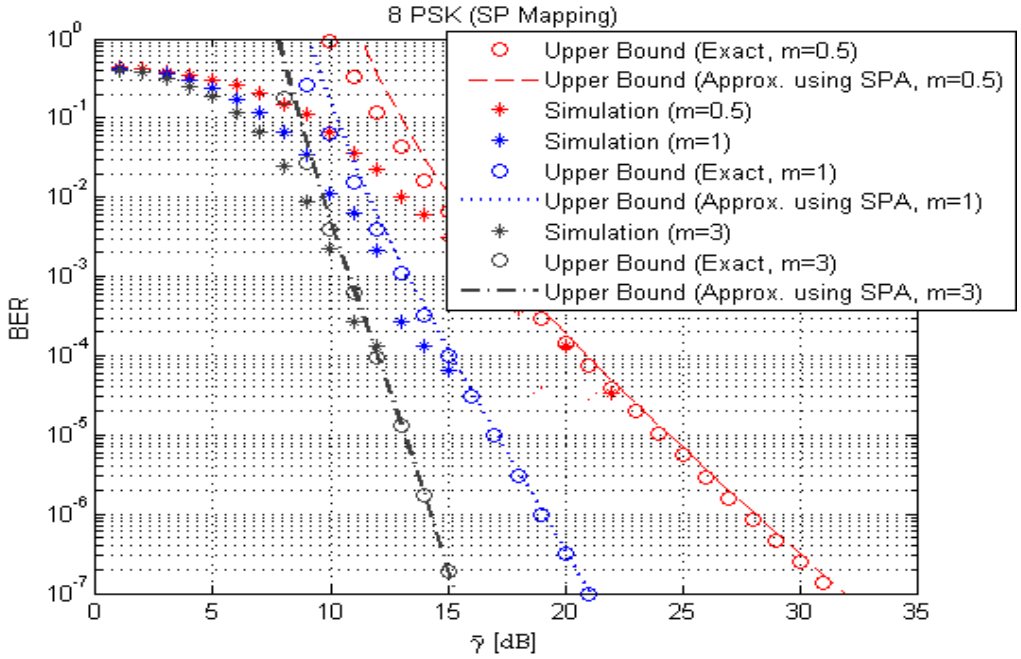

(a)

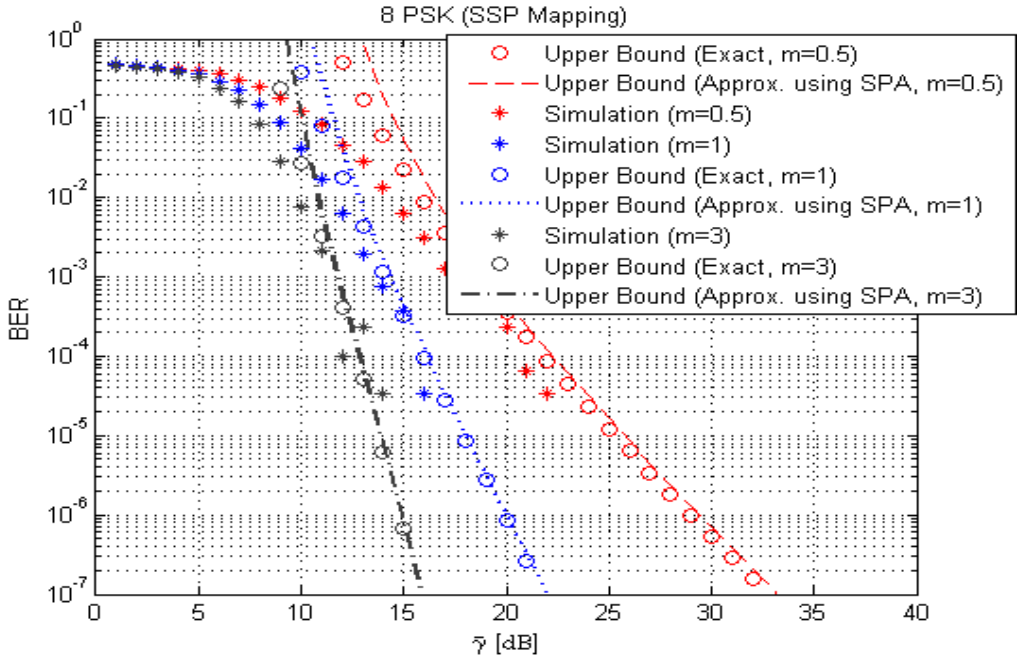

(b)

FIGURE 1.9: BER du BICM sur canal Nakagami-m pour un code convolutionnel de taux $\frac{1}{2}$ pour 8PSK

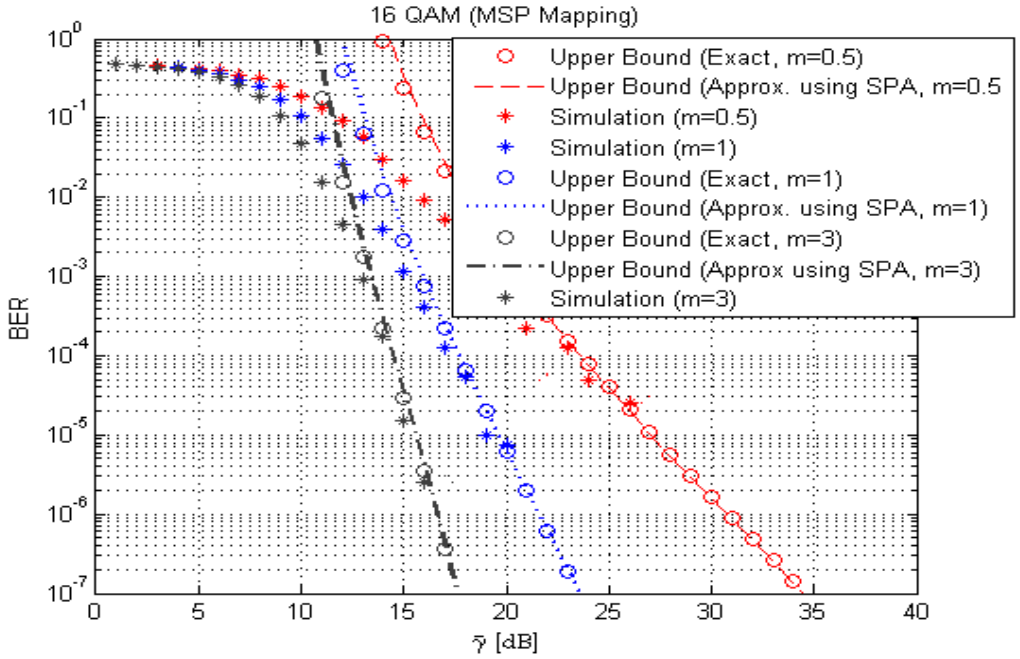

(a)

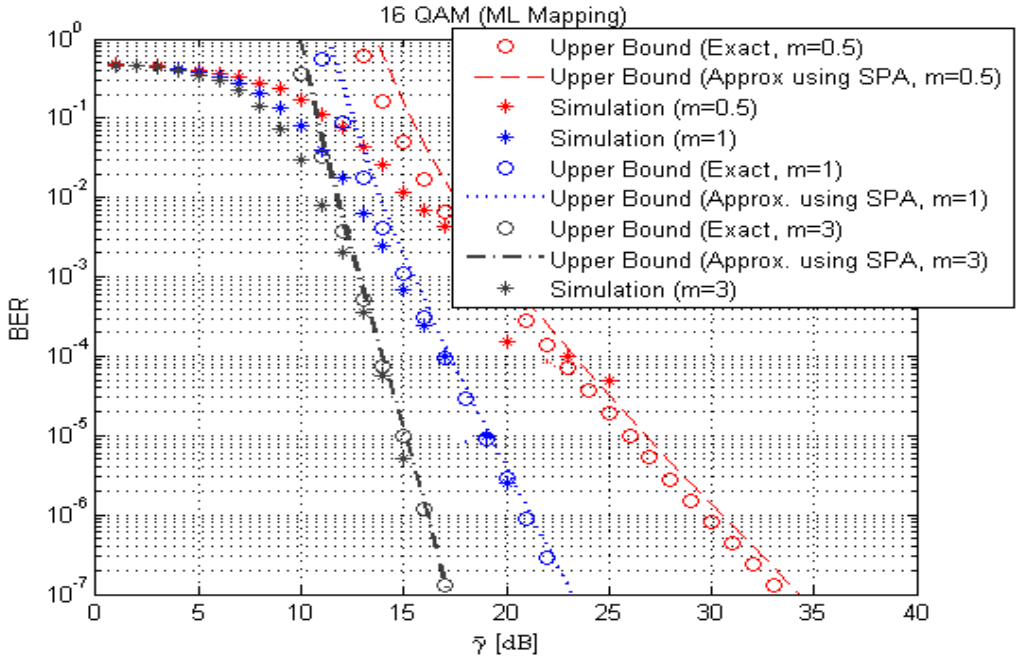

(b)

FIGURE 1.10: BER du BICM sur canal Nakagami-m pour un code convolutionnel de taux $\frac{1}{2}$ pour 16QAM

utilisant la méthode numèrique du modèle exact. On note que la courbe BER obtenue par l′approximation du point de selle et celle obtenue par le modèle exact correspond bien à la simulation. Elles sont presque au dessous de 10^{-4} aux de constellations 8PSK et 16QAM avec étiquetages populaires

1.5 Conclusions

La nouvelle approximation de la PDF des L-values consttituées de quelques termes Gaussiens permet de simplifier l′equation pour calculer la performance. Notre nouvelle approximations est applicable pour le deux constellations QAM et PSK avec étiquetages diffèrents sur des canaux AWGN et Nakagami Fading pour m arbitraire.

Un outil populaire pour calculer BER est l′approximation du point selle. Mais le problème se pose lorsque les métriques non-conformes se mélangent et produisent la fonction polynomial du point selle. Que doit être calculé numériquement. Nous avons dérivé aussi une nouvelle approximation pour trouver le point selle. Les résultats numériques ont confirmé l′exactitude de l′approximation proposée pour le point selle qui est applicable aux constellations QAM et PSK avec étiquetages populaires.

Contents

1 Résumé **iv**

1.1 Introduction iv

1.2 Modèlè de système v

1.2.1 Convention de notation v

1.2.2 Principes de BICM vi

1.2.3 Étiquetages binaires vii

1.2.4 Modèle de Canal vii

1.3 Modèle Probabiliste x

1.3.1 Taux d′erreur d′approximation à l′aide de l′Union Bound . . . xii

1.3.1.1 Résultats numériques xiv

1.4 Approximation du point Selle xvi

1.4.1 Résultats numériques xxi

1.5 Conclusions xxiv

List of Tables **xxviii**

List of Figures **xxix**

2 Introduction **1**

2.1 Contributions 2

2.2 Thesis organization 2

3 System Model **3**

3.1 Notational convention . . . 3

3.2 BICM principles . . . 3

3.3 Binary labelings and Signal Sets . . . 5

3.3.1 Binary labelings . . . 5

3.3.2 Input Alphabets . . . 5

3.4 Channel Models . . . 7

3.4.1 AWGN Channel . . . 7

3.4.2 Fading Channel . . . 8

3.4.2.1 Rayleigh Model . . . 9

3.4.2.2 Nakagami-m Model . . . 9

4 Probabilistic Models of L-values **10**

4.1 Error-Rate Approximation using Union Bound . . . 11

4.2 Approximations for the PDF of L-values . . . 12

4.2.1 Previous Approximations . . . 13

4.3 New Approximation . . . 15

4.3.1 PDF of Reliability metrics(L-values) in Nakagami-m Fading Channel . . . 17

4.3.2 Error rate approximation using Union Bound over AWGN channel 19

4.3.3 Error Rate Approximation using Union Bound over Nakagami-m Fading channel . . . 22

4.4 Numerical Results . . . 23

4.4.1 BER results over AWGN channel . . . 23

4.4.2 BER results over Nakagami-m Fading channel . . . 25

5 Saddle Point Approximation **30**

5.1 New Approximation to find Saddle Point . . . 32

5.2 Numerical Results . . . 34

6 Conclusions **39**

Bibliography **41**

List of Tables

1.1 La fonction de densité de probabilité de fiabilité $f_{L,k|\gamma,d_l}(\lambda)$ et $f_{L,k|\gamma,d_l,\theta_l}(\lambda)$ pour la transmission sur le canal AWGN xi

1.2 Valeurs du coefficient $n_{k,l}$ pour un nombre populaires de constellation et étiquetage. Seuls les coefficients non nuls sont affichés xii

1.3 Nouvelle fonction de densité de probabilité de fiabilité métriques $f_{L,k|\gamma,d_l}(\lambda)$ et $f_{L,k|\gamma,d_l,\theta_l}(\lambda)$ pour la transmission sur le canal AWGN xiv

1.4 La fonction de densité de probabilité de fiabilité métriques $\Phi_{L,k|\gamma,d_l}(s)$, $\Phi_{L,k|\gamma,d_l,\theta_l}(s)$, $\Phi_{L,k|\bar{\gamma},d_l}(s)$, et $\Phi_{L,k|\bar{\gamma},d_l,\theta_l}(s)$ xv

4.1 Probability Density function of reliability metrics $f_{L,k|\gamma,d_l}(\lambda)$ and $f_{L,k|\gamma,d_l,\theta_l}(\lambda)$ for the transmission over AWGN channel 14

4.2 Values of coefficient $n_{k,l}$ for a popular number of constellation and labeling. Only non-zero coefficients are shown 15

4.3 New probability density function of reliability metrics $f_{L,k|\gamma,d_l}(\lambda)$ and $f_{L,k|\gamma,d_l,\theta_l}(\lambda)$ for the transmission over AWGN channel 16

4.4 Probability Density function of reliability metrics $\Phi_{L,k|\gamma,d_l}(s)$, $\Phi_{L,k|\gamma,d_l,\theta_l}(s)$, $\Phi_{L,k|\bar{\gamma},d_l}(s)$,and $\Phi_{L,k|\bar{\gamma},d_l,\theta_l}(s)$ 18

List of Figures

1.1 BICM modéle vi
1.2 (a) Étiquetages Gray et (b) étiquetages Set partitionnement [11] . . . viii
1.3 (a) Étiquetages Modifié Set-partitionnement et (b) étiquetages étiquetage-mixte [12] viii
1.4 BICM canal de transmission x
1.5 Six formations non-équivalentes pour l'ensemble des points de signaux concurrentiels. Le '1' représente le point de signal transmis et les '0' montrent les éléments du point de signal concurrentiel [20] xiii
1.6 BER de la transmission sur le canal AWGN BICM pour un code convolutif de taux de $\frac{1}{2}$ xvii
1.7 BER de la transmission du BICM plus Nakagami-m de canal pour un code de convolution de taux de $\frac{1}{2}$ pour 8 PSK xviii
1.8 BER de la transmission du BICM plus Nakagami-m de canal pour un code de convolution de taux de $\frac{1}{2}$ pour 16 QAM xix
1.9 BER du BICM sur canal Nakagami-m pour un code convolutionnel de taux $\frac{1}{2}$ pour 8PSK xxii
1.10 BER du BICM sur canal Nakagami-m pour un code convolutionnel de taux $\frac{1}{2}$ pour 16QAM xxiii

3.1 BICM model 4
3.2 Gray Mapping and Set partitioning mapping [11] 6
3.3 Modified Set-partitioning mapping and Mixed labeling [12] 6

4.1 BICM transmission channel 10
4.2 Six non-equivalent formations for the set of competitive signal points.The '1' represents the transmitted signal point and '0's show the elements of competitive signal point [20] 13
4.3 BER of BICM transmission over AWGN channel for a convolution code of rate $\frac{1}{2}$ 24
4.4 BER of BICM transmission over Nakagami-m Fading channel(8PSK) 25
4.5 BER of BICM transmission over Nakagami-m channel for a convolution code of rate $\frac{1}{2}$ for 8PSK (SP and SSP) 26
4.6 BER of BICM transmission over Nakagami-m channel for a convolution code of rate $\frac{1}{2}$ for 16 QAM (Gray and SP) 27
4.7 BER of BICM transmission over Nakagami-m channel for a convolution code of rate $\frac{1}{2}$ for 16 QAM (MSP and ML) 28

5.1 BER of BICM transmission over Nakagami-m fading channel for a convolution code of rate $\frac{1}{2}$ of 8 PSK constellation(Gray and SP labeling) 35
5.2 BER of BICM transmission over Nakagami-m fading channel for a convolution code of rate $\frac{1}{2}$ of 8 PSK constellation(SSP labeling) . . . 36
5.3 BER of BICM transmission over Nakagami-m fading channel for a convolution code of rate $\frac{1}{2}$ of 16 QAM constellation(Gray and SP labeling) 37
5.4 BER of BICM transmission over Nakagami-m fading channel for a convolution code of rate $\frac{1}{2}$ of 16 QAM constellation(MSP and ML labeling) 38

Chapter 2

Introduction

Wireless communications is one of the big engineering success stories - not only from a technical point of view, where the progress has been phenomenal but also in terms of the impact on society. Working habits, and even more generally the ways we all communicate, have been changed by the possibility of talking "anywhere, anytime" - answering emails on the go has become an everyday occurrence now.

Behind this emergence, a complex wireless communication system is at work. It follows communication standards, which define how particular elements of the systems are implemented.

Bit-interleaved coded modulation (BICM) is one of the popular modulation technique used in most of the existing wireless communication standards e.g. HSPA [1], IEEE 802.11a/g/n, the DVB standards (DVB-T2 [15], DVB-S2 [16] and DVB-C2 [17]). Other examples include the low complexity receiver proposed by the IEEE for the multiband orthogonal frequency-division multiplexing (OFDM) ultra wideband (UWB) transceiver [8] and the wireless world initiative new radio (WINNER) consortium [14]. BICM-OFDM is also considered as a good candidate for power line communication systems. And it will most likely become part of future standards. Bit-interleaved coded modulation was first introduced by Zehavi in [35] and later

analyzed from an information theory point of view in the landmark paper of Caire et al [11], the major advantage of BICM is its simplicity and flexibility, as a single binary code can be used along with several modulations without further adaptations. BICM maximises the code diversity, therefore is better than trellis coded modulation in fading channel. Moreover, its flexibility and ease of implementation make it popular in non-fading channel too. So, having a clear concept of BICM is necessary for those who intend to improve the efficiency of BICM to fulfil the demand of the future technology.

2.1 Contributions

The main contributions of this thesis are stated below:

• We develop a simplified probabilistic model of reliability metrics (L-values) of BICM transmission that allow for a simple and accurate evaluation of the performance (BER) considering the effect of unequal error protection.

• We propose a simplified model to calculate the saddle point which is one of the key ingredients of so called saddle point approximation to analyze the performance.

2.2 Thesis organization

This chapter serves as a basis for the following chapters. It gives the brief overview of main contribution of the research work.

The remaining part of the thesis is organised in the following order. Chapter 3 discusses about the system model, binary labelings and a brief introduciton of channel models. Chapter 4 focuses on the probabilistic models of reliability metrics (L-values) both in AWGN and Fading Channel. Chapter 5 describes the new approximation to find the saddle point for the so called Saddle point approximations. Finally, the conclusions are drawn in Chapter 6.

Chapter 3

System Model

3.1 Notational convention

In this thesis we use lowercase letter x denote a scalar, and letters $\boldsymbol{x}$ to denote a sequence. The all-zeros and the all-ones vectors are denoted by $\mathbf{0}$ and $\mathbf{1}$, respectively. The set of real numbers is denoted by $\mathbb{R}$. The random variables are denoted by capital letters Y, probabilities by $\Pr\{\cdot\}$, the probability density function (PDF) of the random vector Y by $f(y)$. The expectation of an random variable Y is denoted by $\mathbb{E}(Y)$. A matrix is denoted by $\mathbb{T}$. A symbol set is denoted as $\mathcal{X}$. A Gaussian distribution with mean value μ and variance σ^2 is denoted by $\mathcal{N}_{\mu,\sigma^2}(\lambda)$, and the erf function by $erf(x) \triangleq \frac{2}{\sqrt{\pi}} \int_0^x \exp(-t^2)dt$. The unit step function can be defined as

$$u(x) \triangleq \begin{cases} 1, & x \geq 0 \\ 0, & x < 0 \end{cases}$$

3.2 BICM principles

BICM was first introduced in 1992 in [35] and later it was analyzed by in [11]. A general BICM model is shown in figure 3.1. A BICM model is comprised of binary encoder, a bit interleaver (π) and a memoryless mapper ($\mathcal{M}$) on the transmission side.

The function of mapper $\mathcal{M}$ is to make one-to-one mapping rules that maps the length-m binary random vectors $\boldsymbol{c}' = [c'_1, ..., c'_r]$ to one symbol $\mathcal{X}$, i.e. $\mathcal{M} : \{0,1\}^r \to \mathcal{X}$. The symbols are sent through channel whose output is given by $y = h \cdot x + \eta$ where h is complex channel gain and η is a zero mean, real, white Gaussian noise sample with variance N_0. As the mapping is memoryless, both noise and complex channel gain samples are independent and identically distributed. On the receiver side there is a

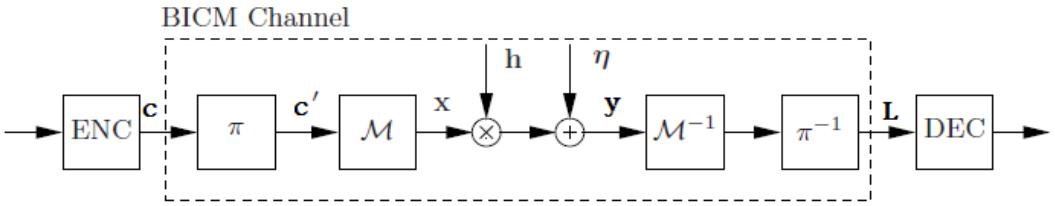

Figure 3.1: BICM model

serial concatenation of de-mapper, de-interleaver and decoder. The received signal at the receiver side will not be the same as the sent symbol because channel will inject some noises in the sending symbol i.e. $y \neq x$. The function of de-mapper is to compute the L-values and then pass to the de-interleaver and at the end decoder. The sign of L-values corresponds to hard decision on the bit and its magnitude represents the reliability of the hard decision. So the L-values are also known as reliability metrics. The reliability metrics calculated by de-mapper $\mathcal{M}^{-1}$ are defined as

$$\hat{L}_j = \log(\frac{\Pr\{c_j = 1|y\}}{\Pr\{c_j = 0|y\}}) \tag{3.1}$$

where y is a received signal, $j = 0, ..., r-1$ is the bit position, and c_j is the j-th bit in the transmitted codeword $\boldsymbol{c} = [c_0, ..., c_{r-1}]$. Using the Bayes' rule it is possible to express the (3.1) as a sum of extrinsic and priori L-values

$$\begin{aligned} \hat{L}_j &= \log(\frac{\Pr\{y|c_j = 1\}}{\Pr\{y|c_j = 1\}}) + \log(\frac{\Pr\{c_j = 1\}}{\Pr\{c_j = 1\}}) \\ &= L_j^{\mathrm{e}} + L_j^{\mathrm{a}} \end{aligned} \tag{3.2}$$

where L_j^{a} is a priori probability. We consider here there is no priori information, i.e. $(L_j^{\mathrm{a}} = 0)$; so

$$\begin{aligned} \hat{L}_j &= \log(\frac{\Pr\{y|c_j = 1\}}{\Pr\{y|c_j = 1\}}) \\ &= \log\{\frac{\sum_{a\epsilon\mathcal{X}_{j,1}} \exp(-\gamma|\frac{y}{h} - a|^2)}{\sum_{a\epsilon\mathcal{X}_{j,0}} \exp(-\gamma|\frac{y}{h} - a|^2)}\} \end{aligned} \tag{3.3}$$

Where $\mathcal{X}_{j,b}$ is the set of symbols with sent bit b at position j. Equation (3.3), simplified using max-log approximation [31], is as follows

$$L_j = \min_{a\epsilon\mathcal{X}_{j,0}}(\gamma|\frac{y}{h} - a|^2) - \min_{a\epsilon\mathcal{X}_{j,1}}(\gamma|\frac{y}{h} - a|^2) \tag{3.4}$$

Although L_j is suboptimal with respect to $\hat{L}_j$, it is known to have small most often negligible impact on the receiver's performance when Gray-mapped constellation are used [27],[3]. This simplification, proposed already in [35],[11] is frequently adopted for ease of the resulting implementation, e.g. by the 3rd generation partnership project (3GPP) working groups [13].

3.3 Binary labelings and Signal Sets

3.3.1 Binary labelings

A binary labeling $\mathbb{T}$ is defined using a matrix of dimensions $M = 2^r$ by r, where each row corresponds to one of the M length-r distinct binary codewords, $\mathbb{L} \triangleq [c_1^T, ..., c_M^T]^T$, where $\boldsymbol{c}_i = [c_{i,1}, c_{i,2}, ..., c_{i,r}]\epsilon\{0,1\}^r$. In this thesis we are particularly interested in Binary reflected gray code (BRGC), Set-partitioning (SP), Modified Set partitioning (MSP) and Mixed-labeling (ML). Figure 3.2, 3.3 show the graphical representation of these popular labelings.

3.3.2 Input Alphabets

Each element of the input alphabet $\mathcal{X}$ is a N-dimensional symbol $x_i, i = 1, ..., M$ where $|\mathcal{X}| = M = 2^r$ and $\mathcal{X} \subset \mathbb{R}^N$. For practical reasons, we are interested in well

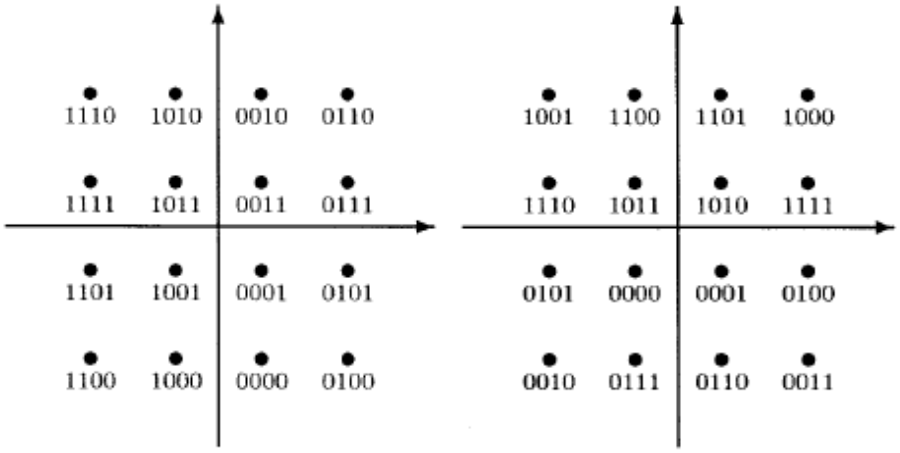

(a) Gray (b) SP

Figure 3.2: Gray Mapping and Set partitioning mapping [11]

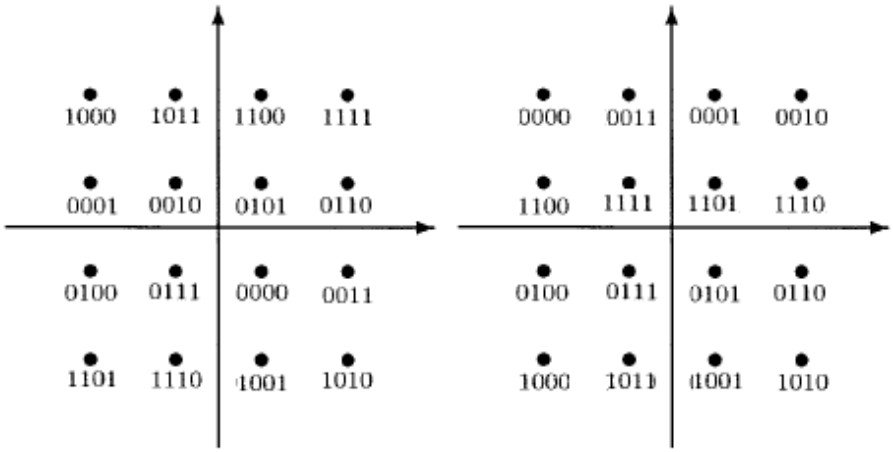

(a) MSP (b) ML

Figure 3.3: Modified Set-partitioning mapping and Mixed labeling [12]

structured discrete input alphabets and we will use the popular M-ary two dimensional input alphabets, i.e., phase-shift keying (M-PSK) and quadrature amplitude modulation (M-QAM).

• An M-PSK symbol set is defined by $\mathcal{X}_{\text{PSK}}$ where $x_i = [\cos(\frac{2\pi i}{M}), \sin(\frac{2\pi i}{M})]$ with $i = 1, ..., M$

• An M-QAM symbol set is defined by the direct product of two $\sqrt{M}-$PAM signal sets where an M-PAM symbol set is defined by $\mathcal{X}_{\text{PAM}}$ where $x_i = -(M - 2i + 1)$ with $i = 1, ..., M$

3.4 Channel Models

In wireless communications the channel is often modelled by a random attenuation (known as fading) of the transmitted signal, followed by additive white Gaussian noise (AWGN). The attenuation term is a simplified form of the underlying physical factors and models the change in signal power over the course of the transmission. The noise in the model are comprised of external interference and/or electronic noise in the receiver. Sometimes noise term is complex to describe the relative time a signal takes to get through the channel. The statistics of the random attenuation are determined by previous measurements or simulations.

3.4.1 AWGN Channel

In the real world, transmission is always affected by noise. The usual mathematical model is AWGN (Additive White Gaussian Noise) channel. It is a well-established model for the physical reality as long as the thermal noise at the receiver is the only source of distribution. The noise is stationary and zero mean Gaussian random process [25]. This means the output of every noise measurement is a zero mean Gaussian random variable that does not depend on the time instant when the measurement

is done. The passband transmit signal x is corrupted by AWGN, resulting in the received signal

$$y = x + \eta$$

where η is a white Gaussian noise, characterised by one sided power spectral density N_0 [28].

3.4.2 Fading Channel

When fading attenuates the signal, the received signal amplitude is modulated by fading amplitude h where h is a random variable with mean value $\mathbb{E}[h^2]$ and the probability density function (PDF) $f_h(h)$ which is dependent on the nature of the radio propagation environment. After passing through the fading channel, the received signal is attenuated at the receiver by Additive white Gaussian noise which is assumed to statistically independent of fading amplitude h. The received signal can be represented as

$$y = h \cdot x + \eta \tag{3.5}$$

where y is the received signal, η is AWGN. Then the signal to noise ratio (SNR) can be defined as

$$\gamma = h^2 \frac{E_s}{N_0}$$

And average signal to noise ratio (SNR) is

$$\bar{\gamma} = \mathbb{E}[h^2] \frac{E_s}{N_0}$$

where E_s is the energy per symbol and $\mathbb{E}[h^2]$ is average fading power. The probability density function of SNR is obtained by introducing a change of variables in the expression for the fading PDF $f_\gamma(\gamma)$, yielding [28]

$$f_\gamma(\gamma) = \frac{f_h(\sqrt{\frac{\mathbb{E}[h^2]\gamma}{\bar{\gamma}}})}{2\sqrt{\frac{\gamma\bar{\gamma}}{\mathbb{E}[h^2]}}} \tag{3.6}$$

and the moment generating function (MGF) $M_\gamma(s)$ is

$$M_\gamma(s) = \int_0^\infty f_\gamma(\gamma) \exp(s\gamma) d\gamma \tag{3.7}$$

3.4.2.1 Rayleigh Model

Rayleigh distribution is used to model multipath fading without line of sight (LOS). The instantaneous SNR per symbol γ is distributed according to the following distribution

$$f_{\bar{\gamma}}(\gamma) = \frac{1}{\bar{\gamma}} \exp(-\frac{\gamma}{\bar{\gamma}}), \gamma \geq 0 \tag{3.8}$$

The MGF corresponding to this fading model can be expressed as

$$M_\gamma(s) = (1 - s\bar{\gamma})^{-1} \tag{3.9}$$

3.4.2.2 Nakagami-m Model

The Nakagami-m probability distribution function can be expressed as SNR per symbol γ which is distributed according to gamma distribution.

$$f_{\bar{\gamma}}(\gamma) = \frac{m^m \gamma^{m-1}}{\bar{\gamma}^m \Gamma(m)} \exp(-\frac{m\gamma}{\bar{\gamma}}) \tag{3.10}$$

It can also be shown that the MGF is given in this case by

$$M_\gamma(s) = (1 - \frac{s\bar{\gamma}}{m})^{-m} \tag{3.11}$$

For instance, it includes the one-sided Gaussian distribution ($m = \frac{1}{2}$) and the Rayleigh distribution ($m = 1$) as special cases. In the limit as $m = \infty$ the Nakagami-m fading channel converges to a nonfading AWGN channel. Finally, the Nakagami-m distribution often gives the best fit to land-mobile [29],[5], and [10] and indoor-mobile [26] multipath propagation, as well as scintillating ionospheric radio links [7],[18],[33],[19], and [6].

Chapter 4

Probabilistic Models of L-values

The L-values can be considered as the output of the BICM channel which is the combination of interleaver, modulator, transmission channel, demodulator and de-interleaver [22] assuming operation with "ideal interleaver", is considered memoryless [35]. Then the knowledge of PDFs of L-values helps to analyze the performance in terms of bit-error rate [22],[2],[23]. The objective of this chapter is to derive the

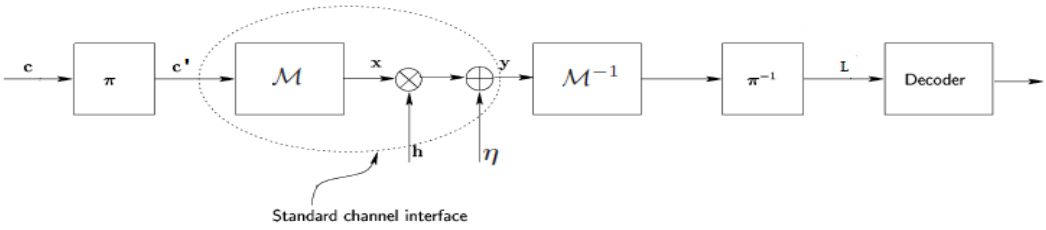

Figure 4.1: BICM transmission channel

probabilistic models of L-values that leads to a simple and accurate evaluation of the performance (BER) of BICM considering the effect of unequal error protection. We can calculate the bounds on the BER in convolutionally-coded transmission to validate the accuracy of the models.

4.1 Error-Rate Approximation using Union Bound

The channel between encoder output c and decoder input L can be considered as equivalent binary input output symmetric (BIOS) channel [22]. Considering maximum likelihood decoding, the error rate of linear codes transmitted over BIOS channel is approximated by union bound [32]. The Union-bound on the BER in convolutionally-coded transmission can be written as [32].

$$P_{\mathrm{b}} \leq UB = \sum_{d=d_{\mathrm{free}}}^{\infty} \beta_d \cdot PEP(d) \tag{4.1}$$

d_{free} is the free distance of the code, β_d is the weight distribution spectrum of the code and $PEP(d)$ is the pairwise error probability which indicates the probability of detecting a codeword with Hamming weight d.

The Pairwise error proabability $PEP(d)$ calculation is based on the decision of the summation of d L-values in the divergent path [4]. Because of the ideal interleaver, L-values are assumed to be independent. So summation of PDF will be the convolution of each PDF. The PDF of L-values conditioned on the sent bit c and SNR γ is denoted by $f_{L|c,\gamma}(\lambda)$. We have

$$f_{L|c,\gamma}^{\sum_d}(\lambda) = f_{L|c,\gamma}(\lambda) * f_{L|c,\gamma}(\lambda) * ... * f_{L|c,\gamma}(\lambda) \tag{4.2}$$

The Pairwise error probability can be calculated by integrating the tail of the PDF.

$$PEP(d) = \int_{-\infty}^{0} f_{L|c,\gamma}^{\sum_d}(\lambda) d\lambda \tag{4.3}$$

A popular approach to calculate the PEP in Nakagami-m Fading channel is to take take the Laplace transform of the PDF of L-values [9]. If $\Phi_{L,c|\bar{\gamma}}(s)$ is the Laplace transform of the PDF of reliability metrics in Fading channel, the mathematical formula to calculate the $PEP(d)$ can be expressed as

$$PEP(d) = \frac{1}{2\pi j} \int_{\alpha-j\infty}^{\alpha+j\infty} [\Phi_{L,c|\bar{\gamma}}(s)]^d \frac{ds}{s} \tag{4.4}$$

where $j \triangleq \sqrt{-1}$ and $\alpha \epsilon \mathbb{R}$ is determined in the region of convergence of the integral. The computation of (4.4) is not straightforward and needs the use of numerical methods [9]. The left hand side of (4.4) is real and so the right hand side must be real and replacing s by $\alpha + j\omega$

$$PEP(d) = \frac{1}{2\pi} \int_{-\infty}^{\infty} \frac{\alpha \Re[\Phi_{L,c|\bar{\gamma}}(\alpha + j\omega)^d] + \omega \Im[\Phi_{L,c|\bar{\gamma}}(\alpha + j\omega)^d]}{\alpha^2 + \omega^2} d\omega \tag{4.5}$$

Gauss-Hermite Integration formula to solve this computation is as follows

$$\int_{-\infty}^{\infty} h(q)dq \simeq \sum_{i=1}^{n} p_i \exp(q_i^2) h(q_i) \tag{4.6}$$

where $h(q) = \exp(-q^2)\Phi_{L,c|\bar{\gamma}}(q)$ and p_i is the weight and n is the total node.

4.2 Approximations for the PDF of L-values

We assume that the channel is symmetric and the code is linear, thus any sequence of bit can be used as a reference. The PDF of L-values can be expressed as the weighted sum of the PDFs $f_{L|j,x,\gamma}(\lambda)$ conditioned on the bit position $1 \leq j \leq r$ and transmitted symbol $x \epsilon \mathcal{X}_{j,1}$ [20]

$$\begin{aligned} f_{L|c=1,\gamma}(\lambda) &= \frac{1}{r} \sum_{j=1}^{r} \sum_{x \epsilon \mathcal{X}_{j,1}} Pr(x|c=b,j) f_{L|j,x,\gamma}(\lambda) \\ &= \frac{1}{r 2^{r-1}} \sum_{k=1}^{r} \sum_{x \epsilon \mathcal{X}_{k,1}} f_{L|j,x,\gamma}(\lambda) \end{aligned} \tag{4.7}$$

where the second step follows from the assumption of the equiprobable modulator input. The main task is to find the expression for $f_{L|j,x,\gamma}(\lambda)$ for every $1 \leq j \leq r$ and $x \epsilon \mathcal{X}_{j,1}$. This needs consideration of all signal points in the constellation and depending on the type of modulation and labeling which actually does not lead to closed form solution.

4.2.1 Previous Approximations

In [11] we notice that $f_{L|j,x,\gamma}(\lambda)$ is approximated by considering all signal points in $\mathcal{X}_{j,\bar{c}}$ for $x\epsilon\mathcal{X}_{j,c}$.

From [11] we know that BICM-EB estimates $f_{L|j,x,\gamma}(\lambda)$ by considering only one member of $\mathcal{X}_{j,\bar{c}}$, which is not a valid simplification for non-gray labeling rules due to presence of multiple nearest neighbours [11],[34], and [22]

In [20] we find the usage of the set of all nearest signal points for a given $x\epsilon\mathcal{X}_{j,c}$ where the set of nearest competitive signal points of x can be mathematically shown as

$$\mathcal{A}_{j,x} \triangleq \left\{a|a\epsilon\mathcal{X}_{j,\bar{c}}, \parallel a-x \parallel = \min_{a'\epsilon\mathcal{A}_{j,\bar{c}}} \parallel a'-x \parallel \triangleq d_{j,x}\right\} \tag{4.8}$$

there are six non-equivalent formations for the set of competitive signal points $\mathcal{A}_{j,x}$ for QAM and PSK constellation and their closed form expression are given in Table 4.1. The PDF of L-values for M-QAM considering the transmission of $c = 1$ while

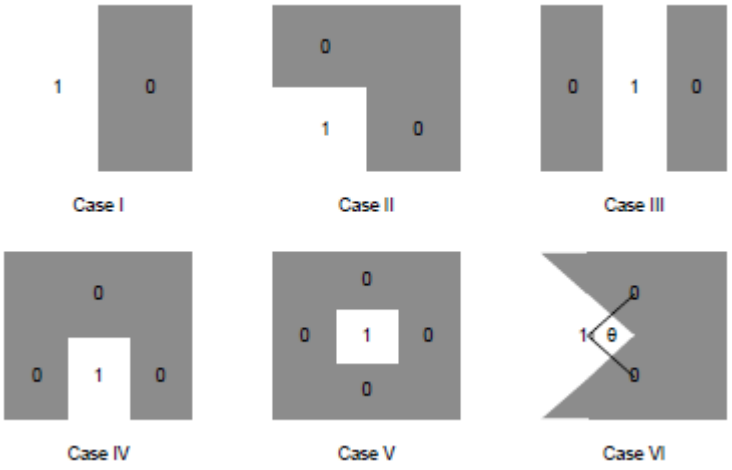

Figure 4.2: Six non-equivalent formations for the set of competitive signal points.The '1' represents the transmitted signal point and '0's show the elements of competitive signal point [20]

replacing the $f_{L|j,x,\gamma}(\lambda)$ in (4.7) by $f_{L,k|\gamma,d_l}(\lambda)$ of Table 4.1, can be expressed as

$$\begin{aligned} f_{L|\gamma}^{\mathrm{QAM}}(\lambda) &= \frac{1}{r2^{r-1}} \sum_{k=1}^{5} \sum_{l=1}^{2^{r-1}-1} n_{k,l} f_{L,k|\gamma,d_l}(\lambda) \\ d_l &= l d_{\min} \end{aligned} \tag{4.9}$$

And the PDF of L-values for M-PSK constellation can be written as

$$\begin{aligned} f_{L|\gamma}^{\mathrm{PSK}}(\lambda) &= \frac{1}{r2^{r-1}} \sum_{l=1}^{2^{r-1}-1} [n_{1,l} f_{L,1|\gamma,d_l}(\lambda) + n_{6,l} f_{L,6|\gamma,d_l,\theta_l}(\lambda)] \\ d_l &= \frac{\sin(\frac{\pi l}{2^r})}{\sin(\frac{\pi}{2^r})} d_{\min} \\ \theta_l &= \pi - \frac{2\pi l}{2^r} \end{aligned} \tag{4.10}$$

The PDFs are calculated considering the subsets of competitive signal points i.e. $c = 0$ at a distance d_l. The coefficient $n_{k,l}$ indicates the number of subsets of type k at an distance d_l. Table 4.2 shows the numerical values of $n_{k,l}$ for well-known constellation and labeling rules. From now on, we use the term "Exact Model" to

Table 4.1: Probability Density function of reliability metrics $f_{L,k|\gamma,d_l}(\lambda)$ and $f_{L,k|\gamma,d_l,\theta_l}(\lambda)$ for the transmission over AWGN channel

$k = 1$	$\mathcal{N}_{d^2\gamma,2d^2\gamma}(\lambda)$
$k = 2$	$\mathcal{N}_{d^2\gamma,2d^2\gamma}(\lambda)(1 - erf(\frac{\lambda - d^2\gamma}{2d\sqrt{\gamma}}))$
$k = 3$	$2\mathcal{N}_{d^2\gamma,2d^2\gamma}(\lambda)u(d^2\gamma - \lambda)$
$k = 4$	$\mathcal{N}_{d^2\gamma,2d^2\gamma}(\lambda)(1 - 2erf(\frac{\lambda - d^2\gamma}{2d\sqrt{\gamma}}))u(d^2\gamma - \lambda)$
$k = 5$	$-4\mathcal{N}_{d^2\gamma,2d^2\gamma}(\lambda)erf(\frac{\lambda - d^2\gamma}{2d\sqrt{\gamma}})u(d^2\gamma - \lambda)$
$k = 6$	$\mathcal{N}_{d^2\gamma,2d^2\gamma}(\lambda)(1 - erf(\tan(\frac{\theta}{2})\frac{\lambda - d^2\gamma}{2d\sqrt{\gamma}}))$

denote the formula shown in Table 4.1. We note that for $k = 1$ the exact model involves only a Gaussian function which is very simple to manipulate i.e. convolution

Table 4.2: Values of coefficient $n_{k,l}$ for a popular number of constellation and labeling. Only non-zero coefficients are shown

4QAM	GL	$n_{1,1} = 4$
	SPL	$n_{1,1} = 2, n_{2,1} = 2$
16QAM	GL	$n_{1,1} = 24, n_{1,2} = 8$
	SPL	$n_{1,1} = 8, n_{1,2} = 4, n_{2,1} = 10, n_{3,1} = 4, n_{4,1} = 4, n_{5,1} = 2$
	MSPL	$n_{1,1} = 16, n_{2,1} = 4, n_{2,2} = 2, n_{3,1} = 4, n_{4,1} = 4, n_{5,1} = 2$
	ML	$n_{1,1} = 24, n_{3,1} = 8$
64QAM	GL	$n_{1,1} = 112, n_{1,2} = 48, n_{1,3} = 16, n_{1,4} = 16$
8PSK	GL	$n_{1,1} = 8, n_{1,2} = 4$
	SPL	$n_{1,1} = 6, n_{1,2} = 2, n_{2,1} = 4$
	SSPL	$n_{1,1} = 6, n_{2,1} = 6$

and integration of Gaussian function are known in closed form. On the other hand, for $k > 1$ the PDFs are Gaussian functions multiplied by corrective factors e.g. erf function, unit step functions. This complicates the analysis of the performance of BICM (calculation of BER etc.).

4.3 New Approximation

The objective of this chapter is to derive new PDFs for these non-equivalent competitive signal points which will be comprised of some Gaussian PDF terms only so it can be easy to analyze the performance of BICM, even in fading channel. We can call it 'Approximate Model' for further reference. The expression for erf function can be approximated as

$$erf(\alpha) \approx \begin{cases} 1 - \exp(-\alpha^2); & \alpha > 0 \\ \exp(-\alpha^2) - 1; & \alpha < 0 \end{cases} \tag{4.11}$$

Since the approximation for erf function in (4.11) depends on the value of the argument, we need to decide which part of the PDF is the most relevant. According to Zero Crossing Model [4], the argument of error function (erf) for $k > 1$ of Table 4.1 are negative. The unit step function in $k = 3, 4, 5$ are not considered as it is approximation to simplify the evaluation. Table 4.3 shows the new PDFs of six non-equivalent subsets of competitive signal points.

Table 4.3: New probability density function of reliability metrics $f_{L,k|\gamma,d_l}(\lambda)$ and $f_{L,k|\gamma,d_l,\theta_l}(\lambda)$ for the transmission over AWGN channel

$k=1$	$\mathcal{N}_{d^2\gamma,2d^2\gamma}(\lambda)$
$k=2$	$2\mathcal{N}_{d^2\gamma,2d^2\gamma}(\lambda) - \frac{1}{\sqrt{2}}\mathcal{N}_{d^2\gamma,d^2\gamma}(\lambda)$
$k=3$	$2\mathcal{N}_{d^2\gamma,2d^2\gamma}(\lambda)$
$k=4$	$3\mathcal{N}_{d^2\gamma,2d^2\gamma}(\lambda) - \sqrt{2}\mathcal{N}_{d^2\gamma,d^2\gamma}(\lambda)$
$k=5$	$4\mathcal{N}_{d^2\gamma,2d^2\gamma}(\lambda) - 2\sqrt{2}\mathcal{N}_{d^2\gamma,d^2\gamma}(\lambda)$
$k=6$	$2\mathcal{N}_{d^2\gamma,2d^2\gamma}(\lambda) - \cos(\frac{\theta}{2})\mathcal{N}_{d^2\gamma,2\cos^2(\frac{\theta}{2})d^2\gamma}(\lambda)$

Now we can consider 16QAM and 8PSK as examples to verify the accuracy of the Approximation model. The PDFs for 16QAM and 8PSK can be derived using (4.9), (4.10), Table 4.2, 4.3 for popular labeling rules.

$$f^{16\text{QAM}}_{L|c=1,\gamma}(\lambda) = \begin{cases} \frac{3}{4}\mathcal{N}_{d_1^2\gamma,2d_1^2\gamma}(\lambda) + \frac{1}{4}\mathcal{N}_{d_2^2\gamma,2d_2^2\gamma}(\lambda); & (GL) \\ \frac{7}{4}\mathcal{N}_{d_1^2\gamma,2d_1^2\gamma}(\lambda) - \frac{13\sqrt{2}}{32}\mathcal{N}_{d_1^2\gamma,d_1^2\gamma}(\lambda) + \frac{1}{8}\mathcal{N}_{d_2^2\gamma,2d_2^2\gamma}(\lambda); & (SPL) \\ \frac{13}{8}\mathcal{N}_{d_1^2\gamma,2d_1^2\gamma}(\lambda) - \frac{5\sqrt{2}}{16}\mathcal{N}_{d_1^2\gamma,d_1^2\gamma}(\lambda) + \frac{1}{8}\mathcal{N}_{d_2^2\gamma,2d_2^2\gamma}(\lambda) - \frac{\sqrt{2}}{32}\mathcal{N}_{d_2^2\gamma,d_2^2\gamma}(\lambda); & (MSPL) \\ \frac{5}{4}\mathcal{N}_{d_1^2\gamma,2d_1^2\gamma}(\lambda); & (ML) \end{cases} \tag{4.12}$$

Where

$$d_1 = d_{\min}; d_2 = 2d_{\min};$$

$$f_{L|c=1,\gamma}^{\text{8PSK}}(\lambda) = \begin{cases} \frac{2}{3}\mathcal{N}_{d_1^2\gamma,2d_1^2\gamma}(\lambda) + \frac{1}{3}\mathcal{N}_{d_2^2\gamma,2d_2^2\gamma}(\lambda); & (GL) \\ \frac{7}{6}\mathcal{N}_{d_1^2\gamma,2d_1^2\gamma}(\lambda) - \frac{\cos(\frac{\theta_1}{2})}{3}\mathcal{N}_{d_1^2\gamma,2\cos^2(\frac{\theta_1}{2})d_1^2\gamma}(\lambda) + \frac{1}{6}\mathcal{N}_{d_2^2\gamma,2d_2^2\gamma}(\lambda); & (SPL) \\ \frac{3}{2}\mathcal{N}_{d_1^2\gamma,2d_1^2\gamma}(\lambda) - \frac{\cos(\frac{\theta_1}{2})}{2}\mathcal{N}_{d_1^2\gamma,2\cos^2(\frac{\theta_1}{2})d_1^2\gamma}(\lambda); & (SSPL) \end{cases} \tag{4.13}$$

Where

$$d_1 = d_{\min}; d_2 = 2\cos(\frac{\pi}{8})d_{\min}; \theta_1 = \frac{3\pi}{4};$$

4.3.1 PDF of Reliability metrics(L-values) in Nakagami-m Fading Channel

The PDF of L-values in Nakagami-m Fading channel can be derived by taking the average over the Nakagami-m distribution. Mathematically it can be expressed as

$$f_{L|c=1,\bar{\gamma}}(\lambda) = \int_0^\infty f_{L|c=1,\gamma}(\lambda) f_{\bar{\gamma}}(\gamma) d\gamma \tag{4.14}$$

where $f_{\gamma|\bar{\gamma}}$ is the PDF of Nakagami-m distribution which can be written as

$$f_{\bar{\gamma}}(\gamma) = \frac{m^m \gamma^{m-1}}{\bar{\gamma}^m \Gamma m} \exp(-\frac{m\gamma}{\bar{\gamma}})$$

For simplification of the performance evaluation of BICM in Nakagami-m Fading channel, it is a common practice to use the Laplace transform of the PDF of L-values.

$$\begin{aligned} \Phi_{L|c=1,\bar{\gamma}}(s) &= \int_{-\infty}^{\infty} f_{L|c=1,\bar{\gamma}}(\lambda) \exp(-s\lambda) d\lambda \\ &= \int_{-\infty}^{\infty} \int_0^\infty f_{L|c=1,\gamma}(\lambda) f_{\bar{\gamma}}(\gamma) \exp(-s\lambda) d\gamma d\lambda \\ &= \int_0^\infty \left(\int_{-\infty}^{\infty} f_{L|c=1,\gamma}(\lambda) \exp(-s\lambda) d\lambda \right) f_{\bar{\gamma}}(\gamma) d\gamma \\ &= \int_0^\infty \Phi_{L|c=1,\gamma}(s) f_{\bar{\gamma}}(\gamma) d\gamma \end{aligned} \tag{4.15}$$

where $\Phi_{L|c=1,\gamma}(s)$ is the Laplace transform of the PDF over AWGN channel and we assume $s\epsilon\mathbb{R}^{+}$. Table 4.4 shows the Laplace transform of the PDFs of six non-equivalent subsets of competitive signal points over AWGN channel and Nakagami-m Fading channel

Table 4.4: Probability Density function of reliability metrics $\Phi_{L,k|\gamma,d_l}(s)$, $\Phi_{L,k|\gamma,d_l,\theta_l}(s)$, $\Phi_{L,k|\bar{\gamma},d_l}(s)$,and $\Phi_{L,k|\bar{\gamma},d_l,\theta_l}(s)$

$k=1$	$\Phi_{L,1\|d,\gamma}(s)$	$\exp(d^2\gamma(s^2-s))$
	$\Phi_{L,1\|d,\bar{\gamma}}(s)$	$\left(\frac{m}{m-d^2\bar{\gamma}(s^2-s)}\right)^m$
$k=2$	$\Phi_{L,2\|d,\gamma}(s)$	$2\exp(d^2\gamma(s^2-s)) - \frac{1}{\sqrt{2}}\exp(d^2\gamma(\frac{s^2}{2}-s))$
	$\Phi_{L,2\|d,\bar{\gamma}}(s)$	$2\left(\frac{m}{m-d^2\bar{\gamma}(s^2-s)}\right)^m - \frac{1}{\sqrt{2}}\left(\frac{m}{m-d^2\bar{\gamma}(\frac{s^2}{2}-s)}\right)^m$
$k=3$	$\Phi_{L,3\|d,\gamma}(s)$	$2\exp(d^2\gamma(s^2-s))$
	$\Phi_{L,3\|d,\bar{\gamma}}(s)$	$2\left(\frac{m}{m-d^2\bar{\gamma}(s^2-s)}\right)^m$
$k=4$	$\Phi_{L,4\|d,\gamma}(s)$	$3\exp(d^2\gamma(s^2-s)) - \sqrt{2}\exp(d^2\gamma(\frac{s^2}{2}-s))$
	$\Phi_{L,4\|d,\bar{\gamma}}(s)$	$3\left(\frac{m}{m-d^2\bar{\gamma}(s^2-s)}\right)^m - \sqrt{2}\left(\frac{m}{m-d^2\bar{\gamma}(\frac{s^2}{2}-s)}\right)^m$
$k=5$	$\Phi_{L,5\|d,\gamma}(s)$	$4\exp(d^2\gamma(s^2-s)) - 2\sqrt{2}\exp(d^2\gamma(\frac{s^2}{2}-s))$
	$\Phi_{L,5\|d,\bar{\gamma}}(s)$	$4\left(\frac{m}{m-d^2\bar{\gamma}(s^2-s)}\right)^m - 2\sqrt{2}\left(\frac{m}{m-d^2\bar{\gamma}(\frac{s^2}{2}-s)}\right)^m$
$k=6$	$\Phi_{L,6\|d,\theta,\gamma}(s)$	$2\exp(d^2\gamma(s^2-s)) - \cos(\frac{\theta}{2})\exp(d^2\gamma(\cos^2(\frac{\theta}{2})s^2-s))$
	$\Phi_{L,6\|d,\theta,\bar{\gamma}}(s)$	$2\left(\frac{m}{m-d^2\bar{\gamma}(s^2-s)}\right)^m - \cos(\frac{\theta}{2})\left(\frac{m}{m-d^2\bar{\gamma}(\cos^2(\frac{\theta}{2})s^2-s)}\right)^m$

The PDFs for 16QAM and 8PSK for Nakagami-m fading channel can be derived from (4.9),and (4.10).

$$\Phi^{16\text{QAM}}_{L|c=1,\bar{\gamma}}(s) = \begin{cases} \frac{3}{4}\left(\frac{m}{m-d_1^2\bar{\gamma}(s^2-s)}\right)^m + \frac{1}{4}\left(\frac{m}{m-d_2^2\bar{\gamma}(s^2-s)}\right)^m; & (GL) \\ \frac{7}{4}\left(\frac{m}{m-d_1^2\bar{\gamma}(s^2-s)}\right)^m - \frac{13\sqrt{2}}{32}\left(\frac{m}{m-d_1^2\bar{\gamma}(\frac{s^2}{2}-s)}\right)^m + \frac{1}{8}\left(\frac{m}{m-d_2^2\bar{\gamma}(s^2-s)}\right)^m; & (SPL) \\ \frac{13}{8}\left(\frac{m}{m-d_1^2\bar{\gamma}(s^2-s)}\right)^m - \frac{5\sqrt{2}}{16}\left(\frac{m}{m-d_1^2\bar{\gamma}(\frac{s^2}{2}-s)}\right)^m & \\ +\frac{1}{8}\left(\frac{m}{m-d_2^2\bar{\gamma}(s^2-s)}\right)^m - \frac{\sqrt{2}}{32}\left(\frac{m}{m-d_2^2\bar{\gamma}(\frac{s^2}{2}-s)}\right)^m; & (MSPL) \\ \frac{5}{4}\left(\frac{m}{m-d_1^2\bar{\gamma}(s^2-s)}\right)^m; & (ML) \end{cases} \tag{4.16}$$

Where

$$d_1 = d_{\min}; d_2 = 2d_{\min};$$

$$\Phi^{8\text{PSK}}_{L|c=1,r\gamma}(s) = \begin{cases} \frac{2}{3}\left(\frac{m}{m-d_1^2\bar{\gamma}(s^2-s)}\right)^m + \frac{1}{3}\left(\frac{m}{m-d_2^2\bar{\gamma}(s^2-s)}\right)^m; & (GL) \\ \frac{7}{6}\left(\frac{m}{m-d_1^2\bar{\gamma}(s^2-s)}\right)^m - \frac{\cos(\frac{\theta_1}{2})}{3}\left(\frac{m}{m-d_1^2\bar{\gamma}(\cos^2(\frac{\theta}{2})s^2-s)}\right)^m + \frac{1}{6}\left(\frac{m}{m-d_2^2\bar{\gamma}(s^2-s)}\right)^m; & (SPL) \\ \frac{3}{2}\left(\frac{m}{m-d_1^2\bar{\gamma}(s^2-s)}\right)^m - \frac{\cos(\frac{\theta_1}{2})}{2}\left(\frac{m}{m-d_1^2\bar{\gamma}(\cos^2(\frac{\theta}{2})s^2-s)}\right)^m; & (SSPL) \end{cases} \tag{4.17}$$

Where

$$d_1 = d_{\min}; d_2 = 2\cos(\frac{\pi}{8})d_{\min}; \theta_1 = \frac{3\pi}{4};$$

4.3.2 Error rate approximation using Union Bound over AWGN channel

The Pairwise error proabability $PEP(d)$ calculation is based on the decision of the summation of d L-values in the divergent path [4]. We assume $d = w_1 + w_2$ then the $PEP(d)$ of 16QAM and 8PSK from (4.12) and (4.13) can be expressed using

binomial series representation for popular labelings as

$$f_{L|c=1,\gamma}^{16\text{QAM},\sum}=\begin{cases}\sum_{i=0}^{w_1}\sum_{k=0}^{w_2}\binom{w_1}{i}\binom{w_2}{k}(\frac{3}{4})^{w_1+w_2-(i+k)}(\frac{1}{4})^{i+k}\times & \\ \mathcal{N}_{(w_1+w_2-i-k)d_1^2\gamma+(i+k)d_2^2\gamma,2((w_1+w_2-i-k)d_1^2\gamma+(i+k)d_2^2\gamma)}(\lambda); & (GL)\\ \sum_{a=0}^{w_1}\sum_{b=0}^{w_1-a}\sum_{c=0}^{w_2}\sum_{d=0}^{w_2-c}\binom{w_1}{a}\binom{w_1-a}{b}\binom{w_2}{c}\binom{w_2-c}{d}\times & \\ (\frac{7}{4})^{w_1+w_2-(a+c+b+d)}(\frac{-13\sqrt{2}}{32})^{b+d}(\frac{1}{8})^{a+c}\times & \\ \mathcal{N}_{(w_1+w_2-a-c)d_1^2\gamma+(a+c)d_2^2\gamma,2((w_1+w_2-a-c-\frac{1}{2}(b+d))d_1^2\gamma+(a+c)d_2^2\gamma)}(\lambda); & (SPL)\\ \sum_{a=0}^{w_1}\sum_{b=0}^{w_1-a}\sum_{c=0}^{a}\sum_{i=0}^{w_2}\sum_{j=0}^{w_2-i}\sum_{k=0}^{i}\binom{w_1}{a}\binom{w_1-a}{b}\binom{a}{c}\binom{w_2}{i}\binom{w_2-i}{j}\binom{i}{k}\times & \\ (\frac{13}{8})^{w_1+w_2-(a+b+i+j)}(\frac{-5\sqrt{2}}{16})^{b+j}(\frac{1}{8})^{a+i-(c+k)}(\frac{-\sqrt{2}}{32})^{c+k}\times & \\ \mathcal{N}_{(w_1+w_2-a-i)d_1^2\gamma+(a+i)d_2^2\gamma,2((w_1+w_2-a-i-\frac{1}{2}(b+j))d_1^2\gamma+(a+i-\frac{1}{2}(c+k))d_2^2\gamma)}(\lambda); & (MSPL)\\ (\frac{5}{4})^{w_1+w_2}\mathcal{N}_{(w_1+w_2)d_1^2\gamma,2(w_1+w_2)d_1^2\gamma}(\lambda); & (ML)\end{cases} \tag{4.18}$$

Where

$$d_1=d_{\min};d_2=2d_{\min};$$

and

$$f_{L|c=1,\gamma}^{8\text{PSK},\sum}=\begin{cases}\sum_{i=0}^{w_1}\sum_{k=0}^{w_2}\binom{w_1}{i}\binom{w_2}{k}\frac{2^{w_1+w_2-(i+k)}}{3^{w_1+w_2}}\times & \\ \mathcal{N}_{((w_1+w_2-i-k)d_1^2+(i+k)d_2^2)\gamma,2((w_1+w_2-i-k)d_1^2+(i+k)d_2^2)\gamma}(\lambda); & (GL)\\ \sum_{a=0}^{w_1}\sum_{b=0}^{w_1-a}\sum_{c=0}^{w_2}\sum_{d=0}^{w_2-c}\binom{w_1}{a}\binom{w_1-a}{b}\binom{w_2}{c}\binom{w_2-c}{d}\times & \\ (\frac{7}{6})^{w_1+w_2-a-c-b-d}(\frac{1}{6})^{a+c}(\frac{-cos(\frac{\theta}{2})}{3})^{b+d}\times & \\ \mathcal{N}_{((w_1+w_2-a-c)d_1^2+(a+c)d_2^2)\gamma,2((w_1+w_2-a-c-(b+d)\sin^2(\frac{\theta}{2}))d_1^2+(a+c)d_2^2)\gamma}(\lambda); & (SPL)\\ \sum_{i=0}^{w_1}\sum_{k=0}^{w_2}\binom{w_1}{i}\binom{w_2}{k}(\frac{3}{2})^{w_1+w_2-i-k}(\frac{-cos(\frac{\theta}{2})}{2})^{i+k}\times & \\ \mathcal{N}_{(w_1+w_2)d_1^2\gamma,2((w_1+w_2-(i+k)\sin^2(\frac{\theta}{2}))d_1^2\gamma}(\lambda); & (SSPL)\end{cases} \tag{4.19}$$

Where

$$d_1=d_{\min};d_2=2\cos(\frac{\pi}{8})d_{\min};\theta_1=\frac{3\pi}{4};$$

The mathematical expressions of $PEP(d)$ for 16QAM and 8PSK using (4.3) are

$$PEP^{16\text{QAM}}_{L|c=1,\gamma}(d) = \begin{cases} \sum_{i=0}^{w_1}\sum_{k=0}^{w_2}\binom{w_1}{i}\binom{w_2}{k}(\frac{3}{4})^{w_1+w_2-(i+k)}(\frac{1}{4})^{i+k}\times \\ \frac{1}{2}[1+erf(-\frac{\sqrt{(w_1+w_2-i-k)d_1^2\gamma+(i+k)d_2^2\gamma}}{2})]; & (GL) \\ \sum_{a=0}^{w_1}\sum_{b=0}^{w_1-a}\sum_{c=0}^{w_2}\sum_{d=0}^{w_2-c}\binom{w_1}{a}\binom{w_1-a}{b}\binom{w_2}{c}\binom{w_2-c}{d}\times \\ (\frac{7}{4})^{w_1+w_2-(a+c+b+d)}(\frac{-13\sqrt{2}}{32})^{b+d}(\frac{1}{8})^{a+c}\times \\ \frac{1}{2}[1+erf(-\frac{(w_1+w_2-a-c)d_1^2\gamma+(a+c)d_2^2\gamma}{2\sqrt{((w_1+w_2-a-c-\frac{1}{2}(b+d))d_1^2\gamma+(a+c)d_2^2\gamma)}})]; & (SPL) \\ \sum_{a=0}^{w_1}\sum_{b=0}^{w_1-a}\sum_{c=0}^{a}\sum_{i=0}^{w_2}\sum_{j=0}^{w_2-i}\sum_{k=0}^{i}\binom{w_1}{a}\binom{w_1-a}{b}\binom{a}{c}\binom{w_2}{i}\binom{w_2-i}{j}\binom{i}{k}\times \\ (\frac{13}{8})^{w_1+w_2-(a+b+i+j)}(\frac{-5\sqrt{2}}{16})^{b+j}(\frac{1}{8})^{a+i-(c+k)}(\frac{-\sqrt{2}}{32})^{c+k}\times \\ \frac{1}{2}[1+erf(-\frac{(w_1+w_2-a-i)d_1^2\gamma+(a+i)d_2^2\gamma}{2\sqrt{((w_1+w_2-a-i-\frac{1}{2}(b+j))d_1^2\gamma+(a+i-\frac{1}{2}(c+k))d_2^2\gamma)}})]; & (MSP) \\ (\frac{5}{4})^{w_1+w_2}\frac{1}{2}[1+erf(-\frac{\sqrt{(w_1+w_2)d_1^2\gamma}}{2})]; & (ML) \end{cases} \tag{4.20}$$

and

$$PEP^{8\text{PSK}}_{L|c=1,\gamma}(d) = \begin{cases} \sum_{i=0}^{w_1}\sum_{k=0}^{w_2}\binom{w_1}{i}\binom{w_2}{k}\frac{2^{w_1+w_2-(i+k)}}{3^{w_1+w_2}}\times \\ \frac{1}{2}[1+erf(-\frac{\sqrt{((w_1+w_2-i-k)d_1^2+(i+k)d_2^2)\gamma}}{2})]; & (GL) \\ \sum_{a=0}^{w_1}\sum_{b=0}^{w_1-a}\sum_{c=0}^{w_2}\sum_{d=0}^{w_2-c}\binom{w_1}{a}\binom{w_1-a}{b}\binom{w_2}{c}\binom{w_2-c}{d}\times \\ (\frac{7}{6})^{w_1+w_2-a-c-b-d}(\frac{1}{6})^{a+c}(\frac{-cos(\frac{\theta}{2})}{3})^{b+d}\times \\ \frac{1}{2}[1+erf(-\frac{((w_1+w_2-a-c)d_1^2+(a+c)d_2^2)\gamma}{2\sqrt{(w_1+w_2-a-c-(b+d)\sin^2(\frac{\theta}{2}))d_1^2+(a+c)d_2^2)\gamma}})]; & (SPL) \\ \sum_{i=0}^{w_1}\sum_{k=0}^{w_2}\binom{w_1}{i}\binom{w_2}{k}(\frac{3}{2})^{w_1+w_2-i-k}(\frac{-cos(\frac{\theta}{2})}{2})^{i+k}\times \\ \frac{1}{2}[1+erf(-\frac{(w_1+w_2)d_1^2\gamma}{2\sqrt{(w_1+w_2-(i+k)\sin^2(\frac{\theta}{2}))d_1^2\gamma}})]; & (SSPL) \end{cases} \tag{4.21}$$

4.3.3 Error Rate Approximation using Union Bound over Nakagami-m Fading channel

Laplace transform of PDF of 16QAM and 8PSK for Nakagami-m Fading channel can be written as

$$\Phi_{L|c=1,\bar{\gamma}}^{16\text{QAM},\sum}(s) = \begin{cases} \sum_{i=0}^{w_1}\sum_{k=0}^{w_2}\binom{w_1}{i}\binom{w_2}{k}\left(\frac{3}{4}\right)^{w_1+w_2-(i+k)}\left(\frac{1}{4}\right)^{i+k}\times \\ \left(\frac{m}{m-d_1^2\bar{\gamma}(s^2-s)}\right)^{(w_1+w_2-i-k)m}\left(\frac{m}{m-d_2^2\bar{\gamma}(s^2-s)}\right)^{(i+k)m}; & (GL) \\ \sum_{a=0}^{w_1}\sum_{b=0}^{w_1-a}\sum_{c=0}^{w_2}\sum_{d=0}^{w_2-c}\binom{w_1}{a}\binom{w_1-a}{b}\binom{w_2}{c}\binom{w_2-c}{d}\times \\ \left(\frac{7}{4}\right)^{w_1+w_2-(a+c+b+d)}\left(\frac{-13\sqrt{2}}{32}\right)^{b+d}\left(\frac{1}{8}\right)^{a+c}\times \\ \left(\frac{m}{m-d_1^2\bar{\gamma}(s^2-s)}\right)^{(w_1+w_2-(a+c+b+d))m}\left(\frac{m}{m-d_1^2\bar{\gamma}(\frac{s^2}{2}-s)}\right)^{(b+d)m}\times \\ \left(\frac{m}{m-d_2^2\bar{\gamma}(s^2-s)}\right)^{(a+c)m}; & (SPL) \\ \sum_{a=0}^{w_1}\sum_{b=0}^{w_1-a}\sum_{c=0}^{a}\sum_{i=0}^{w_2}\sum_{j=0}^{w_2-i}\sum_{k=0}^{i}\binom{w_1}{a}\binom{w_1-a}{b}\binom{a}{c}\binom{w_2}{i}\binom{w_2-i}{j}\binom{i}{k}\times \\ \left(\frac{13}{8}\right)^{w_1+w_2-(a+b+i+j)}\left(\frac{-5\sqrt{2}}{16}\right)^{b+j}\left(\frac{1}{8}\right)^{a+i-(c+k)}\left(\frac{-\sqrt{2}}{32}\right)^{c+k}\times \\ \left(\frac{m}{m-d_1^2\bar{\gamma}(s^2-s)}\right)^{(w_1+w_2-(a+b+i+j))m}\left(\frac{m}{m-d_1^2\bar{\gamma}(\frac{s^2}{2}-s)}\right)^{(b+j)m}\times \\ \left(\frac{m}{m-d_2^2\bar{\gamma}(s^2-s)}\right)^{(a+i-(c+k))m}\left(\frac{m}{m-d_2^2\bar{\gamma}(\frac{s^2}{2}-s)}\right)^{(c+k)m}; & (MSPL) \\ \left(\frac{5}{4}\right)^{w_1+w_2}\left(\frac{m}{m-d_1^2\bar{\gamma}(s^2-s)}\right)^{(w_1+w_2)m}; & (ML) \end{cases} \tag{4.22}$$

$$\Phi^{8\text{PSK},\sum}_{L|c=1,\gamma}(s) = \begin{cases} \sum_{i=0}^{w_1}\sum_{k=0}^{w_2}\binom{w_1}{i}\binom{w_2}{k}\frac{2^{w_1+w_2-(i+k)}}{3^{w_1+w_2}}\times \\ \left(\frac{m}{m-d_1^2\bar{\gamma}(s^2-s)}\right)^{(w_1+w_2-(i+k))m}\left(\frac{m}{m-d_2^2\bar{\gamma}(s^2-s)}\right)^{(i+k)m}; & (GL) \\ \sum_{a=0}^{w_1}\sum_{b=0}^{w_1-a}\sum_{c=0}^{w_2}\sum_{d=0}^{w_2-c}\binom{w_1}{a}\binom{w_1-a}{b}\binom{w_2}{c}\binom{w_2-c}{d}\times \\ \left(\frac{7}{6}\right)^{w_1+w_2-a-c-b-d}\left(\frac{1}{6}\right)^{a+c}\left(\frac{-cos(\frac{\theta}{2})}{3}\right)^{b+d}\times \\ \left(\frac{m}{m-d_1^2\bar{\gamma}(s^2-s)}\right)^{(w_1+w_2-a-c-b-d)m}\left(\frac{m}{m-d_1^2\bar{\gamma}(\cos^2\frac{\theta}{2}s^2-s)}\right)^{(b+d)m}\times \\ \left(\frac{m}{m-d_2^2\bar{\gamma}(s^2-s)}\right)^{(a+c)m}; & (SPL) \\ \sum_{i=0}^{w_1}\sum_{k=0}^{w_2}\binom{w_1}{i}\binom{w_2}{k}\left(\frac{3}{2}\right)^{w_1+w_2-i-k}\left(\frac{-cos(\frac{\theta}{2})}{2}\right)^{i+k}\times \\ \left(\frac{m}{m-d_1^2\bar{\gamma}(s^2-s)}\right)^{(w_1+w_2-i-k)m}\left(\frac{m}{m-d_1^2\bar{\gamma}(\cos^2\frac{\theta}{2}s^2-s)}\right)^{(i+k)m}; & (SSPL) \end{cases} \tag{4.23}$$

4.4 Numerical Results

In this section, we show the numerical results to compare with the exact model so it can prove the accuracy of the proposed approximation. To calculate the BER, we assume BICM with rate $\frac{1}{2}$ convolution code with generator polynomials $[5\ 7]_8$ with constraint length $K = 3$. First we consider the BER results over AWGN channel, after the BER results for Nakagami-m fading channel

4.4.1 BER results over AWGN channel

We show the comparison between simulated result and analytical results (Exact model and Approximate Model) as a function of SNR γ. To calculate the BER Union bound, we consider first 20 terms of the distance spectrum of the convolution code. Figure 4.3 shows the simulated and analytical (Exact model and Approximate model) BER results for 8PSK and 16QAM constellations and popular labelings for transmission over AWGN channel. We notice that the BER union bound is fairly tight between the exact model and the approximate model in almost all SNR region

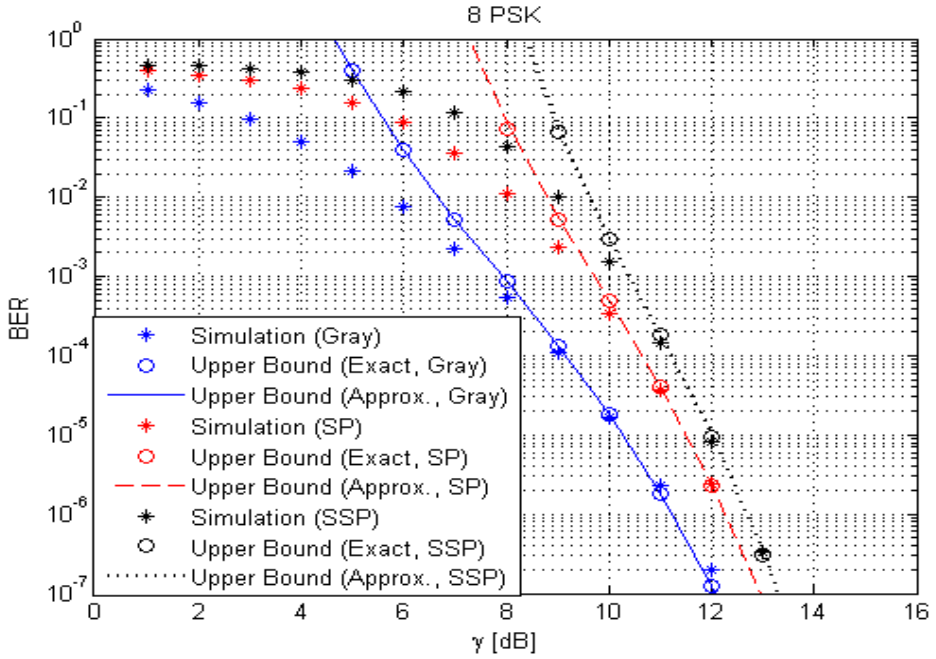

(a)

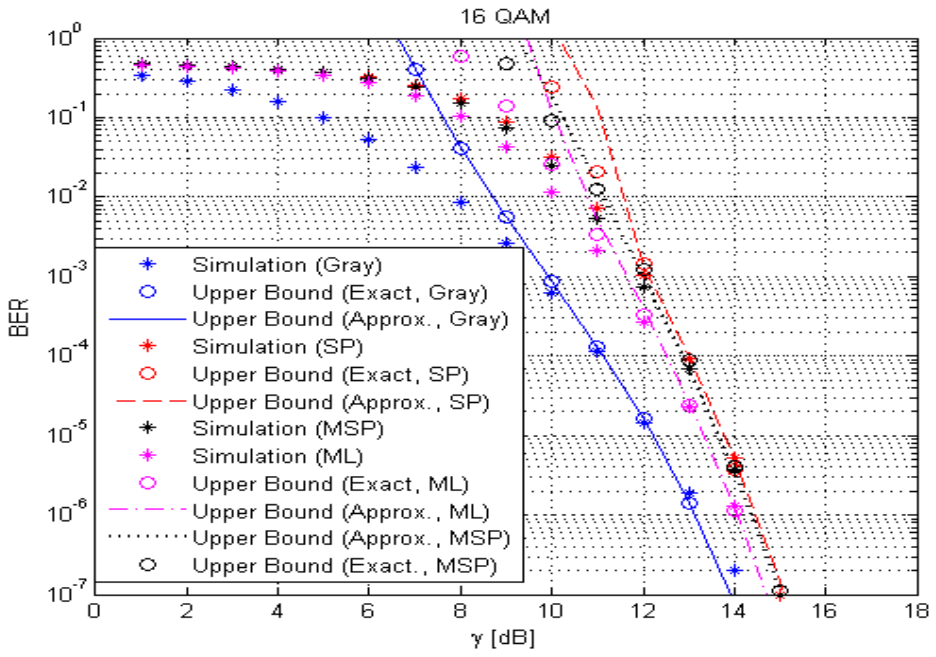

(b)

Figure 4.3: BER of BICM transmission over AWGN channel for a convolution code of rate $\frac{1}{2}$

and in case of the simulated results it is especially below about 10^{-4}. Especially for Gray mapping, the approximate model has a tight upper bound below 10^{-2} because the PDF of L-values for gray mapping are purely Gaussian function. So Approximate model predicts well the error rate performance of BICM over AWGN channel.

4.4.2 BER results over Nakagami-m Fading channel

Now we show the comparison between simulated result and analytical results (Exact model and Approximate Model) as a function of SNR $\bar{\gamma}$ over Nakagami-m Fading channel. To calculate the BER Union bound, we consider first 20 terms of the distance spectrum of the convolution code. Fig. 4.4-4.7 show the simulated and analytical

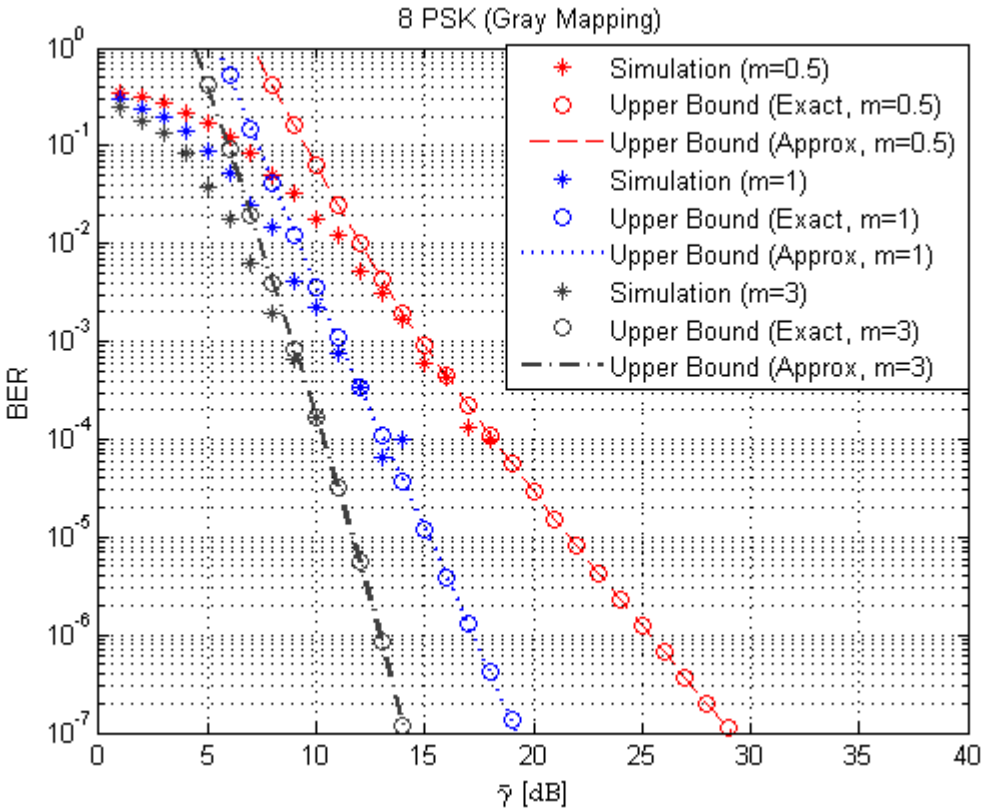

Figure 4.4: BER of BICM transmission over Nakagami-m Fading channel(8PSK)

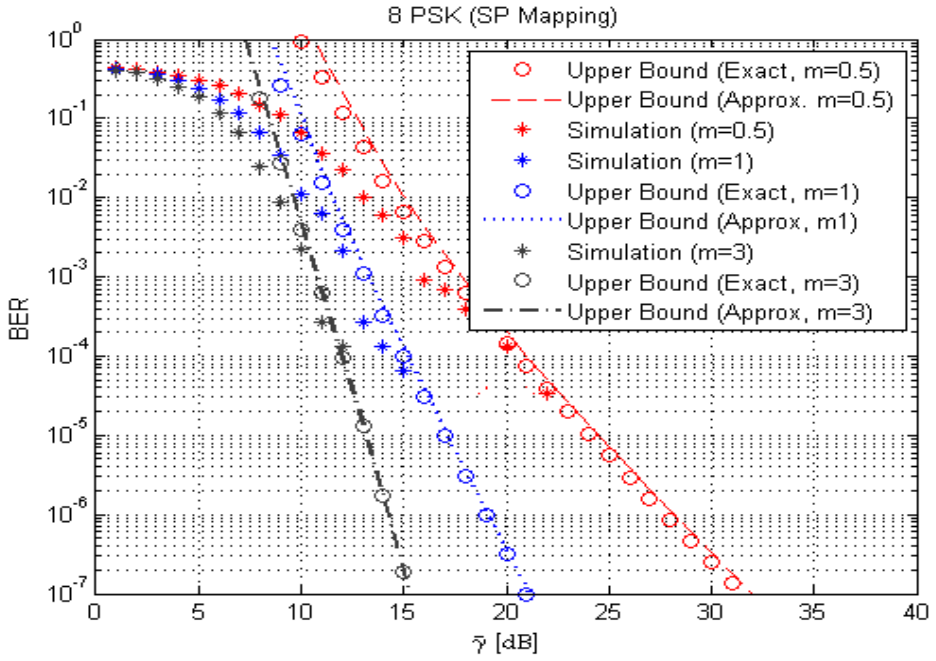

(a)

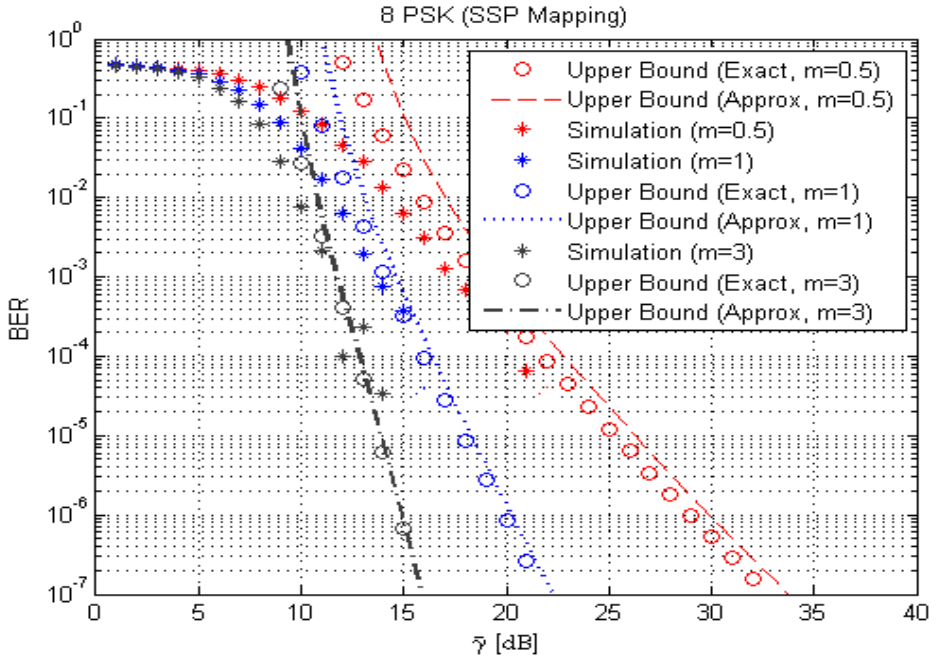

(b)

Figure 4.5: BER of BICM transmission over Nakagami-m channel for a convolution code of rate $\frac{1}{2}$ for 8PSK (SP and SSP)

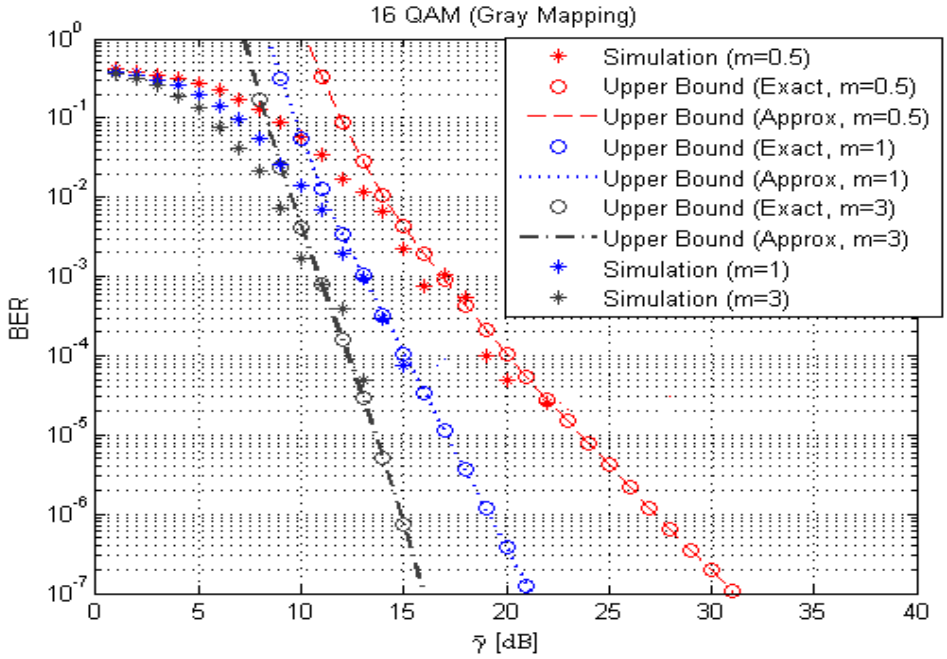

(a)

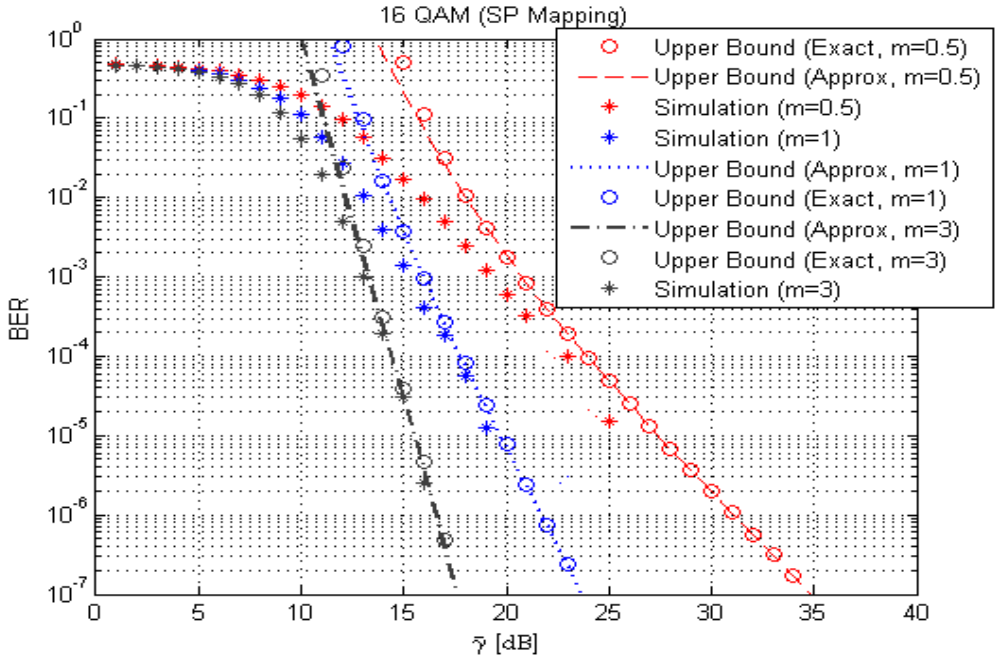

(b)

Figure 4.6: BER of BICM transmission over Nakagami-m channel for a convolution code of rate $\frac{1}{2}$ for 16 QAM (Gray and SP)

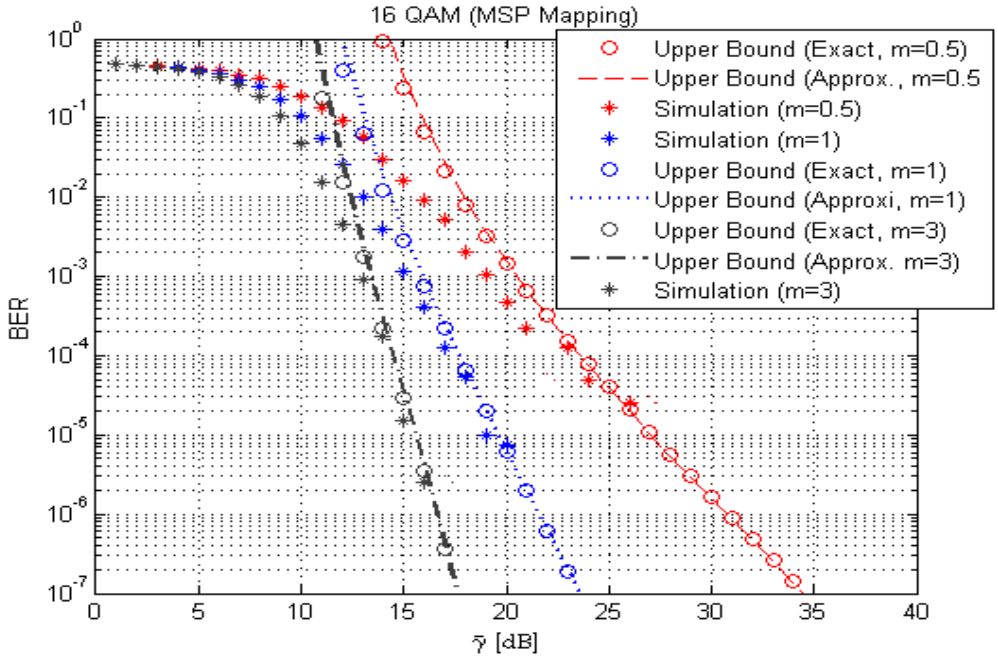

(a)

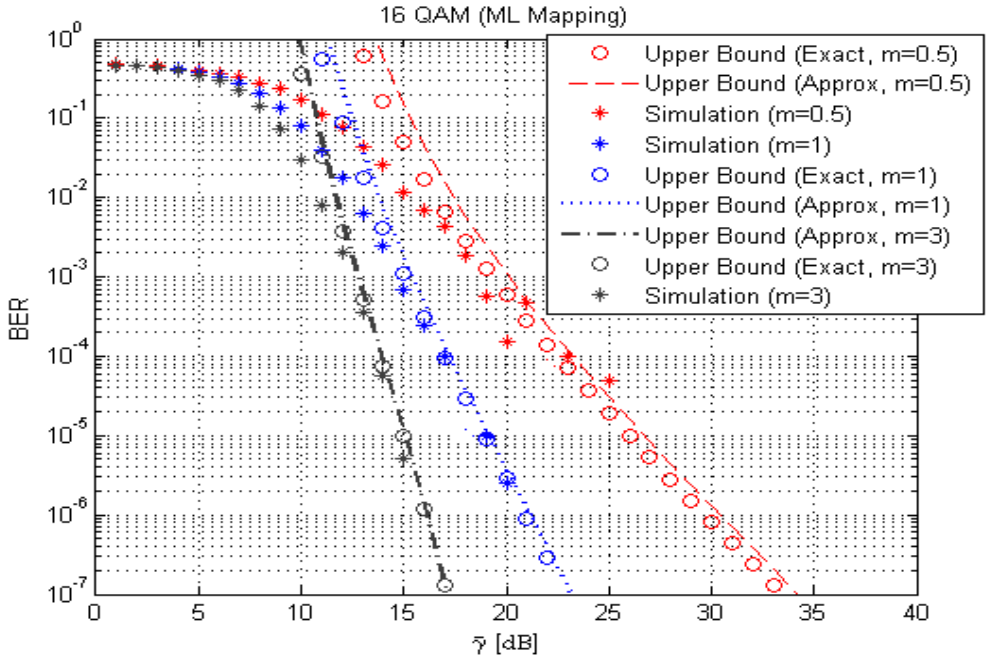

(b)

Figure 4.7: BER of BICM transmission over Nakagami-m channel for a convolution code of rate $\frac{1}{2}$ for 16 QAM (MSP and ML)

(Exact model and Approximate model) BER results for 8PSK and 16QAM constellations and popular labelings for transmission over Nakagami-m channel. We notice that the BER union bound is tight between the exact model and the approximate model in almost all SNR region and in case of the simulated results it is especially below about 10^{-4}. For the Gray mapping, the approximate model has a tight upper bound below 10^{-2} because the PDF of L-values for gray mapping follows Gaussian distribution.The simulation for different constellations are not close to each other because each constellation is based on nearest neighbour where Gray mapping has the optimal value. SP mapping converges faster than SSP mapping. So Approximate model predicts well the error rate performance of BICM over Nakagami-m Fading channel.

Chapter 5

Saddle Point Approximation

BER estimation [32] is based on the code spectrum and the expression of the Pair-wise error probability $PEP(d)$ between two codewords [21] where d is the Hamming distance. PEP can be expressed as the tail probability of random variable generated by adding d LLRs $L_1, L_2, ..., L_d$. It can be written by choosing the all-one codeword;

$$PEP(d) = Pr(L^{\sum_d} \triangleq \sum_{i=1}^{d} L_i < 0) \tag{5.1}$$

From (4.2) we notice that summation of L-values is the convolution of each PDF of L-values. A general approach to solve this problem is to take the Laplace transform of each PDF and multiply to get the total PDF of L-values. So the Laplace transform of total PDF of L-values can be expressed as

$$\begin{aligned} \Phi_{d|\bar{\gamma}}^{\sum_d}(s) &= \prod_{i=1}^{d} \Phi_{d|L_i,\bar{\gamma}}(s) \\ &= [\Phi_{d|L,\bar{\gamma}}(s)]^d \end{aligned}$$

Where $\Phi_{d|L,\bar{\gamma}}(s)$ is the laplace transform of each L-values. A general method to solve this computation has been discussed in section 4.1. In [9] a few bounds and estimation have been proposed among which saddle point approximation has got the attention due to its simple form and accuracy [11],[22]. The mathematical expression

to calculate the saddle point approximation can be written as

$$PEP(d) = \frac{\exp(\kappa_{d|\bar{\gamma}}(\hat{s}))}{\hat{s}\sqrt{2\pi\kappa^{''}_{d|\bar{\gamma}}(\hat{s})}} \tag{5.2}$$

where $\kappa_{d|\bar{\gamma}}(s)$ is cumulant generating function and $\hat{s}$ is the so-called saddle point solving $\kappa'_{d|\bar{\gamma}}(\hat{s}) = 0$

$$\kappa_{d|\bar{\gamma}}(s) = d\log(\Phi_{d|L,\bar{\gamma}}(s)) \tag{5.3}$$

The first derivative of $\kappa_{d|\bar{\gamma}}(s)$ with respect to s can be written as

$$\kappa^{'}_{d|\bar{\gamma}}(s) = \frac{d\Phi^{'}_{d|L,\bar{\gamma}}(s)}{\Phi_{d|L,\bar{\gamma}}} \tag{5.4}$$

And the second derivative of $\kappa_{d|\bar{\gamma}}(s)$

$$\kappa^{''}_{d|\bar{\gamma}}(s) = \frac{d\Phi^{''}_{d|L,\bar{\gamma}}(s)}{\Phi_{d|L,\bar{\gamma}}(s)} - \frac{d[\Phi^{'}_{d|L,\bar{\gamma}}(s)]^2}{[\Phi_{d|L_i,\bar{\gamma}(s)}]^2} \tag{5.5}$$

Since $\kappa^{'}_{d|\bar{\gamma}}(\hat{s}) = 0$ then $\Phi^{'}_{d|L,\bar{\gamma}}(\hat{s}) = 0$. So

$$\kappa^{''}_{d|\bar{\gamma}}(\hat{s}) = \frac{d\Phi^{''}_{d|L,\bar{\gamma}}(\hat{s})}{\Phi_{d|L,\bar{\gamma}}(\hat{s})} \tag{5.6}$$

Replacing the value of $\kappa_{d|\bar{\gamma}}(\hat{s})$ and $\kappa^{''}_{d|\bar{\gamma}}(\hat{s})$ in (5.2) $PEP(d)$ can be expressed as

$$PEP(d) = \frac{[\Phi_{d|L,\bar{\gamma}}(\hat{s})]^{d+\frac{1}{2}}}{\hat{s}\sqrt{2\pi\Phi^{''}_{d|L,\bar{\gamma}}(\hat{s})}} \tag{5.7}$$

While (5.7) seems simple, the most complicated part is to find the saddle point $\hat{s}$. To have a better insight into the problem, we can consider the PDF of reliability metrics of 16QAM modulation for Gray mapping from (4.12).

$$\begin{aligned}
\kappa^{'}_{d|\bar{\gamma}}(s) &= \frac{d}{ds}\kappa_{d|\bar{\gamma}}(s) = \frac{d}{ds}\log(\Phi^{\text{16QAM}}_{L|c=1,\bar{\gamma}}(s)) \\
&= \frac{d}{ds}\log\left(\frac{3}{4}\left(\frac{m}{m-d_1^2\bar{\gamma}(s^2-s)}\right)^m + \frac{1}{4}\left(\frac{m}{m-d_2^2\bar{\gamma}(s^2-s)}\right)^m\right) \\
&= \frac{\frac{3d_1^2\bar{\gamma}(2s-1)(m-d_2^2(s^2-s)^{m+1}+d_2^2\bar{\gamma}(2s-1)(m-d_1^2\bar{\gamma}(s^2-s))^{m+1}}{(m-d_1^2\bar{\gamma}(s^2-s))^{m+1}(m-d_2^2(s^2-s)^{m+1}}}{\left(\frac{3}{4}\left(\frac{m}{m-d_1^2\bar{\gamma}(s^2-s)}\right)^m + \frac{1}{4}\left(\frac{m}{m-d_2^2\bar{\gamma}(s^2-s)}\right)^m\right)}
\end{aligned} \tag{5.8}$$

According to saddle point approximation we need to solve,

$$\begin{aligned}\kappa^{'}_{d|\bar{\gamma}}(\hat{s}) &= \Phi^{'}_{d|L,\bar{\gamma}}(\hat{s}) \\ &= \frac{3d_1^2\bar{\gamma}(2\hat{s}-1)(m-d_2^2(\hat{s}^2-\hat{s})^{m+1}+d_2^2\bar{\gamma}(2\hat{s}-1)(m-d_1^2\bar{\gamma}(\hat{s}^2-\hat{s}))^{m+1}}{(m-d_1^2\bar{\gamma}(\hat{s}^2-\hat{s}))^{m+1}(m-d_2^2(\hat{s}^2-\hat{s})^{m+1}} \\ &= 0\end{aligned} \tag{5.9}$$

Since the mathematical expression is a polynomial function of $\hat{s}$, thus the closed form solution does not exist in general and $\Phi^{'}_{d|L,\bar{\gamma}}(\hat{s})$ is a convex function [30]; we can solve this problem using fast search method to find the saddle point [20] which is unique.

5.1 New Approximation to find Saddle Point

From (4.9),(4.10),(4.12), and (4.13) we know that the total PDF of reliability metrics are comprised of more than one Gaussian components. If the Laplace transform of the total PDF is $\Phi_{d|L,\bar{\gamma}}(s)$ and Gaussian terms in the total PDF are $\Phi_1(s), ..., \Phi_n(s)$ then the mathematical expression of Laplace transform of the total PDF can be written as

$$\Phi_{d|L,\bar{\gamma}}(s) = \sum_{i=1}^{n} \Phi_i(s) \tag{5.10}$$

According to saddle point approximation, $\kappa^{'}(\hat{s}) = \Phi^{'}_{d|L,\bar{\gamma}}(\hat{s}) = 0$. So we need to solve

$$\sum_{i=1}^{n} \Phi^{'}_i(\hat{s}) = 0 \tag{5.11}$$

Instead of solving it directly, which may be difficult as we explained we proposed the approximation to simplify the problem. Now if we consider $\hat{s}_i$ is the saddle point by setting the first derivative of i-th Laplace transform of Gaussian term $\Phi^{'}_i(\hat{s}_i) = 0$ then according to Taylor's theorem [24]

$$\Phi^{'}_i(\hat{s}) \approx \Phi^{'}_i(\hat{s}_i) + (\hat{s}-\hat{s}_i)\Phi^{''}_i(\hat{s}_i) \tag{5.12}$$

Replacing the value of $\Phi_i^{'}(\hat{s})$ in (5.11) we get

$$\begin{aligned}\sum_{i=1}^{n}(\hat{s}-\hat{s}_i)\Phi_i^{''}(\hat{s}_i)&=0\\ \hat{s}&=\frac{\sum_{i=1}^{n}\hat{s}_i\Phi_i^{''}(\hat{s}_i)}{\sum_{i=1}^{n}\Phi_i^{''}(\hat{s}_i)}\end{aligned} \tag{5.13}$$

To explain the approximation, we can consider 16QAM. The PDF and the Laplace transform of the PDF for SP labeling. From (4.12),(4.16) we get

$$f^{16\text{QAM}}(\lambda)=\frac{7}{4}\mathcal{N}_{d_1^2\gamma,2d_1^2\gamma}(\lambda)-\frac{13\sqrt{2}}{32}\mathcal{N}_{d_1^2\gamma,d_1^2\gamma}(\lambda)+\frac{1}{8}\mathcal{N}_{d_2^2\gamma,2d_2^2\gamma}(\lambda)$$

$$\Phi^{16\text{QAM}}(s)=\frac{7}{4}\left(\frac{m}{m-d_1^2\bar{\gamma}(s^2-s)}\right)^m-\frac{13\sqrt{2}}{32}\left(\frac{m}{m-d_1^2\bar{\gamma}(\frac{s^2}{2}-s)}\right)^m+\frac{1}{8}\left(\frac{m}{m-d_2^2\bar{\gamma}(s^2-s)}\right)^m \tag{5.14}$$

From this expression, according to the approximation we consider each Gaussian term as a separate PDF.

$$\begin{aligned}\Phi_1(s)&=\frac{7}{4}\left(\frac{m}{m-d_1^2\bar{\gamma}(s^2-s)}\right)^m\\ \Phi_2(s)&=-\frac{13\sqrt{2}}{32}\left(\frac{m}{m-d_1^2\bar{\gamma}(\frac{s^2}{2}-s)}\right)^m\\ \Phi_3(s)&=\frac{1}{8}\left(\frac{m}{m-d_2^2\bar{\gamma}(s^2-s)}\right)^m\end{aligned} \tag{5.15}$$

The first and second derivative of (5.15) with respect to s can be expressed as

$$\begin{aligned}\Phi_1^{'}(s)&=\frac{7}{4}\frac{m^{m+1}d_1^2\bar{\gamma}(2s-1)}{(m-d_1^2\bar{\gamma}(s^2-s))^{m+1}};\\ \Phi_2^{'}(s)&=-\frac{13\sqrt{2}}{32}\frac{m^{m+1}d_1^2\bar{\gamma}(s-1)}{(m-d_1^2\bar{\gamma}(\frac{s^2}{2}-s))^{m+1}};\\ \Phi_3^{'}(s)&=\frac{1}{8}\frac{m^{m+1}d_2^2\bar{\gamma}(2s-1)}{(m-d_2^2\bar{\gamma}(s^2-s))^{m+1}};\\ \Phi_1^{''}(s)&=\frac{7}{4}m^{m+1}\left(\frac{2d_1^2\bar{\gamma}}{(m-d_1^2\bar{\gamma}(s^2-s))^{m+1}}+\frac{(m+1)(d_1^2\bar{\gamma}(2s-1))^2}{(m-d_1^2\bar{\gamma}(s^2-s))^{m+2}}\right);\\ \Phi_2^{''}(s)&=-\frac{13\sqrt{2}}{32}m^{m+1}\left(\frac{d_1^2\bar{\gamma}}{(m-d_1^2\bar{\gamma}(\frac{s^2}{2}-s))^{m+1}}+\frac{(m+1)(d_1^2\bar{\gamma}(s-1))^2}{(m-d_1^2\bar{\gamma}(\frac{s^2}{2}-s))^{m+2}}\right);\\ \Phi_3^{''}(s)&=\frac{1}{8}m^{m+1}\left(\frac{2d_2^2\bar{\gamma}}{(m-d_2^2\bar{\gamma}(s^2-s))^{m+1}}+\frac{(m+1)(d_2^2\bar{\gamma}(2s-1))^2}{(m-d_2^2\bar{\gamma}(s^2-s))^{m+2}}\right);\end{aligned} \tag{5.16}$$

Setting the first derivative to zero, we can get the saddle points of individual cumulant generating function which can be defined as $\hat{s}_1 = \frac{1}{2}, \hat{s}_2 = 1$ and $\hat{s}_3 = \frac{1}{2}$. We can get the new saddle point of the total PDF using (5.13)

$$\hat{s} = \frac{\hat{s}_1\Phi_1''(\hat{s}_1) + \hat{s}_2\Phi_2''(\hat{s}_2) + \hat{s}_3\Phi_3''(\hat{s}_3)}{\Phi_1''(\hat{s}_1) + \Phi_2''(\hat{s}_2) + \Phi_3''(\hat{s}_3)} \tag{5.17}$$

5.2 Numerical Results

In this section, we show the numerical results to prove the accuracy of the proposed approximation to calculate the saddle point for saddle point approximation which is a popular method to compute the pairwise error probability (PEP). For performance analysis, we assume BICM with rate $\frac{1}{2}$ convolution code with generator polynomials $[5\ 7]_8$ with constraint length $K = 3$.

Figure 5.1 and Figure 5.2 show that BER curves are obtained using saddle point approximation with new approximation to find saddle point and using numerical method for exact model. We notice a good match between BER curve obtained by saddle point approximation and exact model and it matches well with simulation. They almost overlap below 10^{-3} in case of 8PSK constellation with popular labelings

Figure 5.3 and Figure 5.4 show that BER curves are obtained using saddle point approximation with new approximation to find saddle point and using numerical method for exact model. We notice a tight bound between BER curve obtained by saddle point approximation and exact model and it matches well with simulation. They almost overlap below 10^{-4} in case of 16QAM constellation with popular labelings.

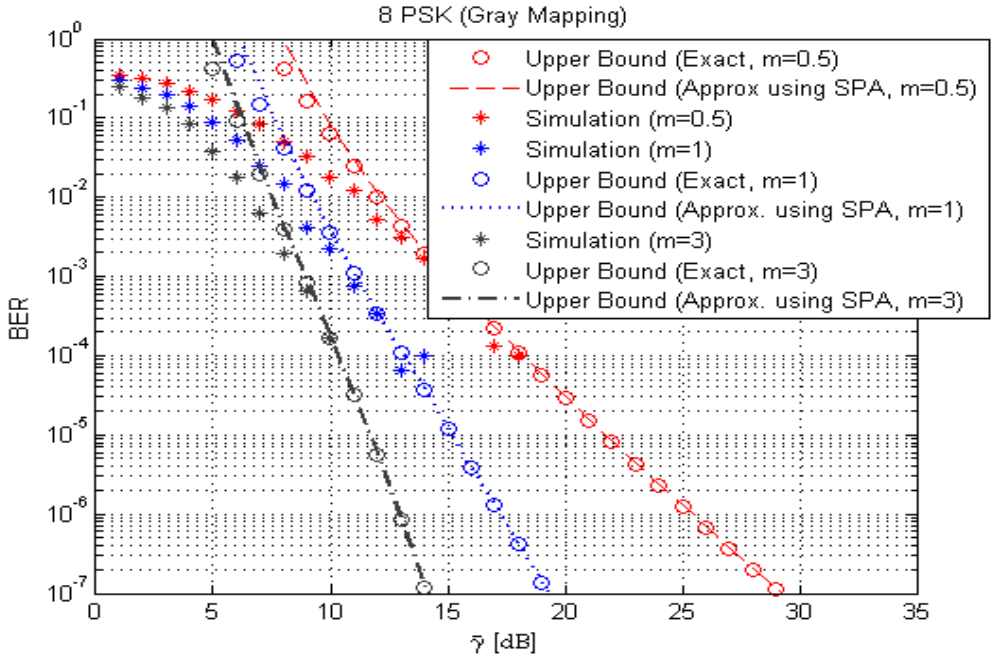

(a)

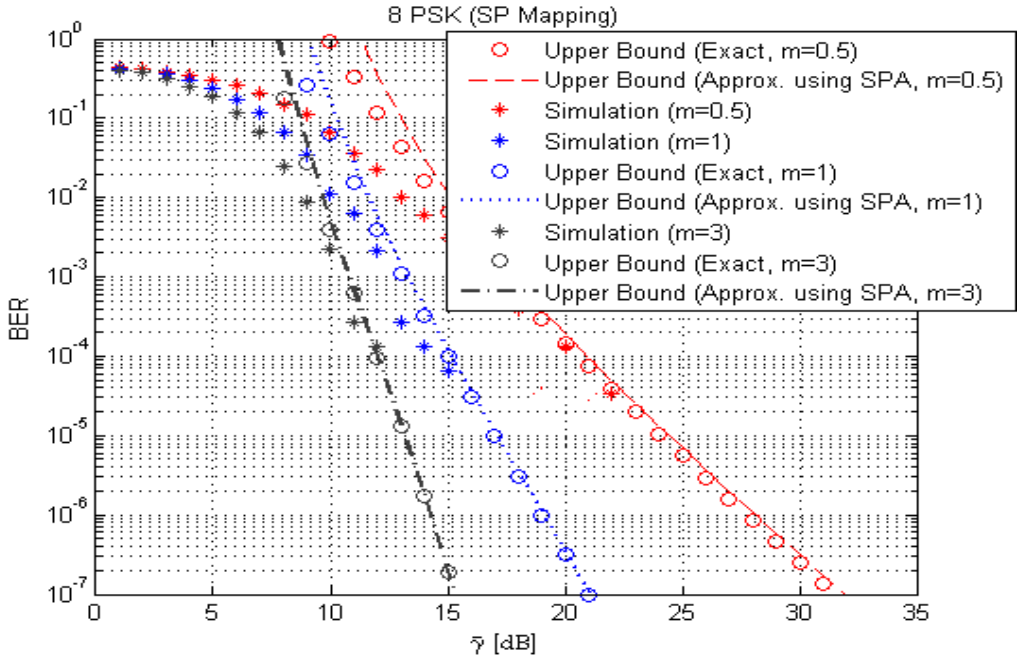

(b)

Figure 5.1: BER of BICM transmission over Nakagami-m fading channel for a convolution code of rate $\frac{1}{2}$ of 8 PSK constellation(Gray and SP labeling)

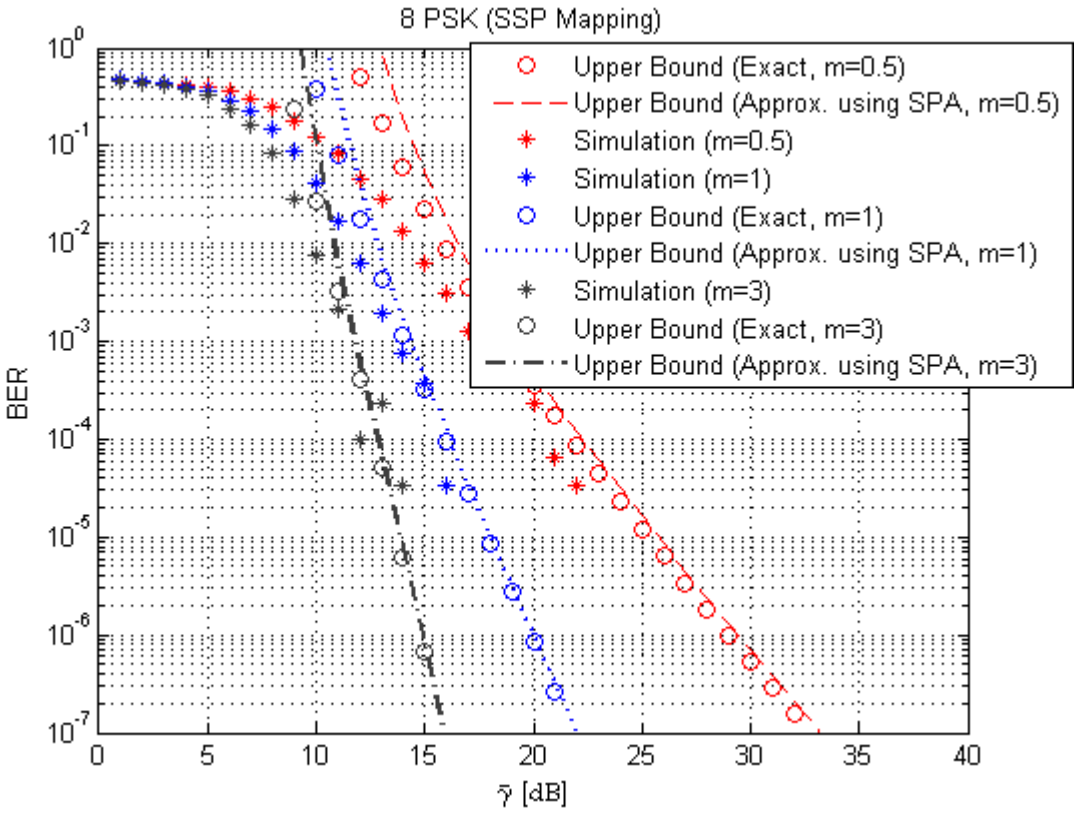

Figure 5.2: BER of BICM transmission over Nakagami-m fading channel for a convolution code of rate $\frac{1}{2}$ of 8 PSK constellation(SSP labeling)

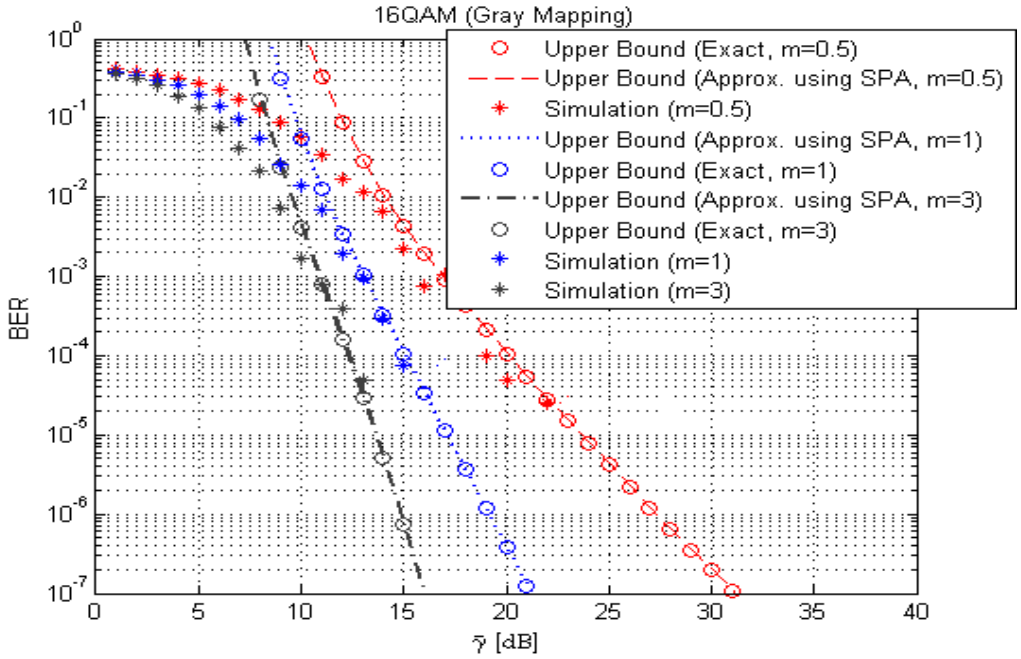

(a)

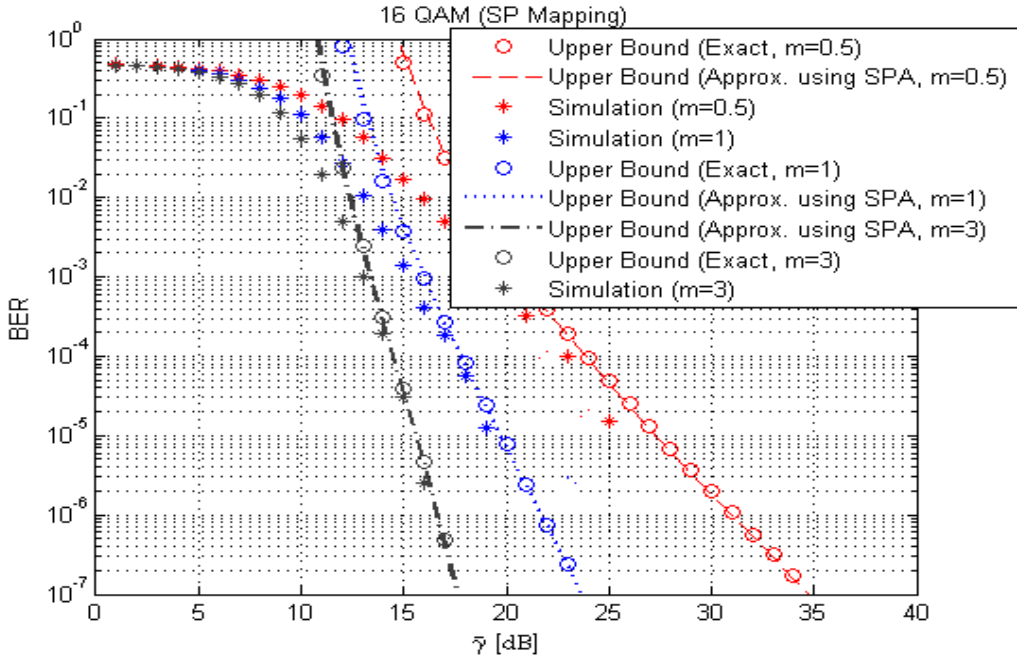

(b)

Figure 5.3: BER of BICM transmission over Nakagami-m fading channel for a convolution code of rate $\frac{1}{2}$ of 16 QAM constellation(Gray and SP labeling)

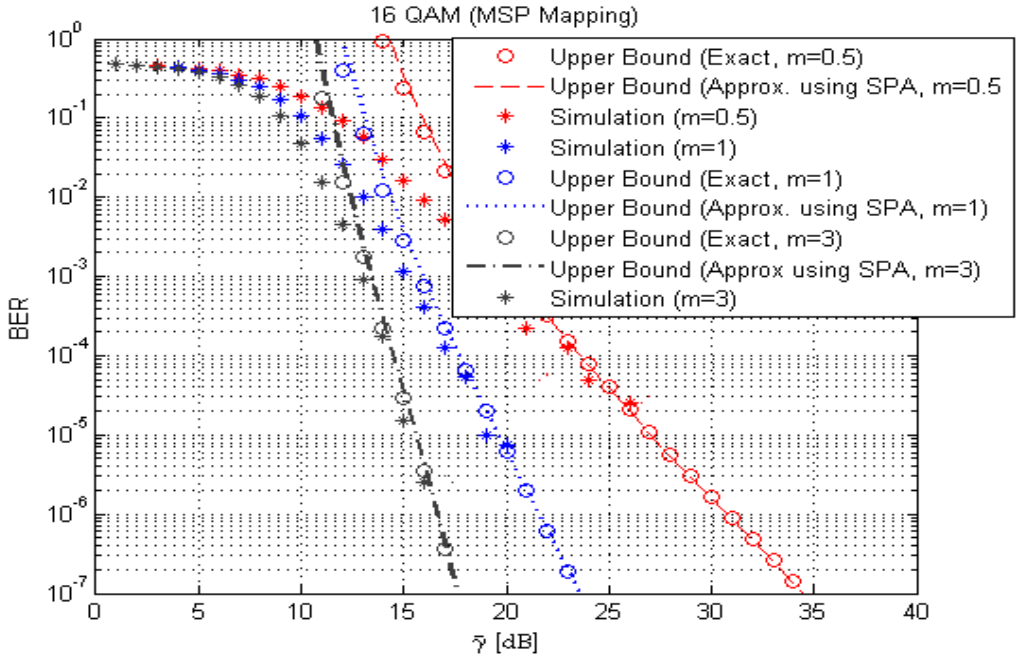

(a)

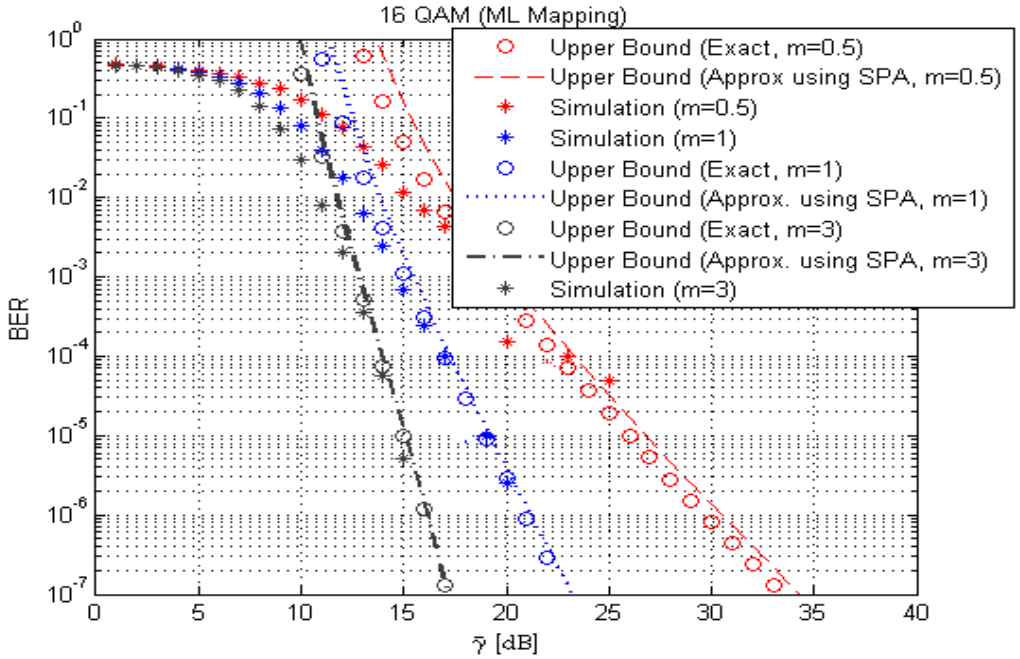

(b)

Figure 5.4: BER of BICM transmission over Nakagami-m fading channel for a convolution code of rate $\frac{1}{2}$ of 16 QAM constellation(MSP and ML labeling)

Chapter 6

Conclusions

BICM is a popular and efficient coded modulation whose analysis is of great importance. The main goal of this work was to propose a method that allow for a simple and accurate evaluation of the performance (BER) considering the effect of unequal error protection in BICM receiver. To this end, we have developed a new approximate model of PDFs of L-values and for the sake of simplified analysis, we also have presented a new approximation to find the saddle point for the so-called saddle point approximation which is a powerful tool to evaluate the performance of BICM. The advantage over [20] is that we do not need Appell's double Hypergeometric function and Gauss' Hypergeometric function to get the simplified form because the approximation, consists of simple Gaussian terms.

Thus the main contribution of this thesis are as follows:

• The new approximation of the PDF of L-values is proposed. It consists in using solely Gaussian terms which makes the performance analysis simple. This new approximation lets us also to obtain the closed form expressions in Nakagami-m Fading channel. Our new approximations are applicable to both QAM and PSK constellations with different labelings over AWGN and Nakagami-m fading channels for arbitrary m. Numerical results have also confirmed the accuracy of the proposed

approximations for SNR regions of interest for convolutionally coded BICM.

• We have also derived a new approximation to find the saddle point. The presented numerical results confirmed the accuracy of the proposed approximation for the saddle point which is applicable to QAM and PSK constellation with all popular labelings.

Bibliography

[1] 3GPP, "Universal mobile telecommunications system (UMTS); multiplexing and channel coding (FDD)," 3GPP, TS 125.212, V7.11.0 Release 7, 2009.

[2] A. Abedi and A. K. Khandani, "An analytical method for approximate performance evaluation of binary linear block codes," *IEEE Trans. Commun.*, vol. 52, no. 2, pp. 228–235, Feb. 2004.

[3] A. Alvarado, H. Carrasco, and R. Feick, "On adaptive BICM with finite blocklength and simplified metrics calculation," in *IEEE. Veh.Technol. Conf. 2006 (VTC-2006 Fall)*, Montreal, Canada, Sep. 2006.

[4] A. Alvarado, L. Szczecinski, R. Feick, and L. Ahumada, "Distribution of L-values in gray-mapped M^2-QAM: Closed-Form Approximations and Applications," *IEEE Trans. Commun.*, vol. 57, no. 7, pp. 2071–2079, Jul. 2009.

[5] T. Aulin, "Characteristics of a digital mobile radio channel," *IEEE Trans. Veh. Technol.*, vol. VT-30, pp. 45–53, May 1981.

[6] P. K. Banerjee, R. S. Dabas, and B. M. Reddy, *C-band and L-band transionospheric scintillation experiment: some results for applications to satellite radio systems.* Radio Sci., Jun. 1992, vol. 27, pp. 955–969.

[7] S. Basu, E. M. MacKenzie, E. Costa, P. F. Fougere, H. C. Carlson, and H. E. Whitney, "250 Mhz/Ghz scintillation parameters in the equatorial, polar, and aural environments," *IEEE J. Sel. Areas Commun.*, vol. SAC-5, pp. 102–115, Feb. 1987.

[8] A. Batra, "Multi-band OFDM physical layer proposal for IEEE 802.15 task group 3a," http://grouper.ieee.org/groups/802/15/, Mar. 2004, document IEEE P802.15-03/268r3.

[9] E. Biglieri, G. Caire, G. Taricco, and J. Ventura-Traveset, "Computing error probabilities over fading channels: a unified approach," *Eur. Trans. Telecommun.*, vol. 9, no. 1, pp. 15–25, Jan./Feb. 1998.

[10] W. R. Braun and U. Dersch, "A physical mobile radio channel model," *IEEE Trans. Veh. Technol.*, vol. VT-40, pp. 472–482, May 1991.

[11] G. Caire, G. Taricco, and E. Biglieri, "Bit-interleaved coded modulation," *IEEE Trans. Inf. Theory*, vol. 44, no. 3, pp. 927–946, May 1998.

[12] A. Chindapol and J. A. Ritcey, "Design, Analysis, and Performance Evaluation for BICM-ID with Square QAM constellations in Rayleigh Fading Channels," *IEEE journal Sel. areas communi.*, vol. 19, no. 5, pp. 944–957, May 2001.

[13] Ericsson, Motorola, and Nokia, "Link evaluation methods for high speed downlink packet access (HSDPA)," Ericsson, Motorola, and Nokia, TSG-RAN Working Group 1 Meeting 15 TSGR1-15(00)1093, Aug. 2000.

[14] T. L. et al., "D2.2.3 modulation and coding schemes for the WINNER II system," https://www.ist-winner.org, WINNER II, Tech. Rep. IST-4-027756, Nov. 2007.

[15] ETSI, "Digital video broadcasting (DVB); Frame structure channel coding and modulation for a second generation digital terrestrial television broadcasting system (DVB-T2)," ETSI, Tech. Rep. ETSI EN 302 755 V1.1.1 (2009-09), Sep. 2009.

[16] ——, "Digital video broadcasting (DVB); Second generation framing structure, channel coding and modulation systems for broadcasting, interactive services, news gathering and other broadband satellite applications (DVB-S2)," ETSI, Tech. Rep. ETSI EN 302 307 V1.2.1 (2009-08), Aug. 2009.

[17] ——, "Digital video broadcasting (DVB); Frame structure channel coding and modulation for a second generation digital transmission system for cable system (DVB-C2)," ETSI, Tech. Rep. ETSI EN 302 769 V1.1.1 (2010-04), Apr. 2010.

[18] E. J. Fremouw and H. F. Bates, *Worldwide behavior of average VHF UHF scintillation.* Radio Sci., Oct. 1971, vol. 6, pp. 1095–1104.

[19] E. J. Fremouw, R. C. Livingston, and D. A. Miller, "On the statistics of scintillating signals," *J. Atmos. Terr. Phys.*, vol. 42, pp. 717–731, Aug. 1980.

[20] A. Kenarsari-Anhari and L. Lampe, "An Analytical Approach for Performance Evaluation of BICM Transmission over Nakagami-m Fading Channels," *IEEE Trans. Communi.*, vol. 58, no. 4, pp. 1090–1101, Apr. 2010.

[21] ——, "Performance Analysis for BICM Transmission over Gaussian Mixture Noise Fading Channels," *IEEE Trans. Communi.*, 2010.

[22] A. Martinez, A. G. i Fabregas, and G. Caire, "Error probability analysis of bit-interleaved coded modulation," *IEEE Trans. Inform. Theory*, vol. 52, no. 1, pp. 262–271, Jan. 2006.

[23] ——, "A closed-form approximation for the error probability of BPSK fading channels," *IEEE Trans. Wireless Commun.*, vol. 6, no. 6, pp. 2051–2054, Jun. 2007.

[24] W. Rudin, *Principles of mathematical analysis.* McGraw-Hill, 1976.

[25] H. Schulze and C. Luders, *Theory and Applications of OFDM and CDMA Wideband Wireless Communications.* John Wiley and Sons Ltd, 2005.

[26] A. U. Sheikh, M. Handforth, and M. Abdi, "Indoor mobile radio channel at 946 Mhz: measurements and modeling," in *IEEE Veh. Technol. Conf. (VTC93)*, Secaucus, NJ, May 1993, pp. 73–76.

[27] M. K. Simon and R. Annavajjala, "On the optimality of bit detection of certain digital modulations," *IEEE Trans. Commun.*, vol. 53, no. 2, pp. 299–307, Feb. 2005.

[28] M. K. Simon and M.-S. Alouini, *Digital Communication over Fading Channels: A Unified Approach to Performance Analysis.* John Wiley and Sons, Inc., 2000.

[29] H. Suzuki, "A statistical model for urban multipath propagation," *IEEE Trans. Commun.*, vol. COM-25, pp. 673–680, Jul. 1977.

[30] L. Szczecinski, A. Alvarado, and R. Feick, "Distribution of maxlog metrics for QAM-based BICM in fading channels," *IEEE Trans. Commun.*, 2009.

[31] A. J. Viterbi, "An intuitive justification and a simplified implementation of the MAP decoder for convolutional codes," *IEEE J. Sel. Areas Commun.*, vol. 16, no. 2, pp. 260–264, Feb. 1998.

[32] A. J. Viterbi and J. K. Omura, *Principles of Digital Communication and Coding.* New York: McGraw-Hill, Inc., 1979.

[33] H. E. Whitney, J. Aarons, R. S. Allen, and D. R. Seeman, *Estimation of the cumulative probability distribution function of ionospheric scintillations.* Radio Sci., Dec. 1972, vol. 7, pp. 1095–1104.

[34] P. Yeh, S. Zummo, and W. Stark, "Error probability of bit-interleaved coded modulation in wireless environments," *IEEE Trans. Veh. Technol.*, vol. 55, no. 2, p. 722728, Mar. 2006.

[35] E. Zehavi, "8-PSK trellis codes for a Rayleigh channel," *IEEE Trans. Commun.*, vol. 40, no. 3, pp. 873–884, May 1992.